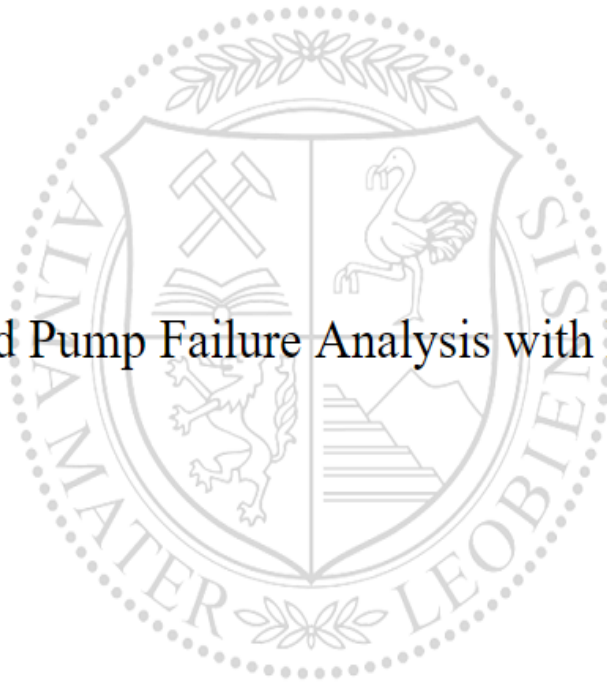




Chair of Petroleum and Geothermal Energy Recovery

Master's Thesis

Smart Sucker Rod Pump Failure Analysis with Machine Learning



Ameni Ben Smida, BSc

March 2019


AFFIDAVIT

I declare on oath that I wrote this thesis independently, did not use other than the specified sources and aids, and did not otherwise use any unauthorized aids.

I declare that I have read, understood, and complied with the guidelines of the senate of the Montanuniversität Leoben for "Good Scientific Practice".

Furthermore, I declare that the electronic and printed version of the submitted thesis are identical, both, formally and with regard to content.

Date 08.03.2019



Signature Author
Ameni, Ben Smida
Matriculation Number: 01435467

Danksagung / Acknowledgement

Primarily, I am grateful to the God for the good health and wellbeing that were necessary to complete my master thesis.

I place on record, my sincere thank you to my university advisors Dipl.-Ing.Dr.Mont Rudolf Fruhwirth and DDI.Dr.mont Langbauer Clemens. I am extremely thankful and indebted to them for sharing expertise, and valuable guidance and encouragement extended to me.

I take this opportunity to express gratitude to all myrconn solutions company members for their help and support especially the manager Michael Stundner and the company consultant for data analysis Georg Pözlbauer. I would like to express my deepest thanks and appreciation for their extremely helpful advice, continuous guidance, and encouragement in creating this work. Simply, without their kind helps, this work would not come to light.

I also thank my parents and sisters for the unceasing encouragement, support and attention.

Kurzfassung

Gestängetiefpumpen ist das am häufigsten verwendete künstliche Förderverfahren zur Steigerung der Ölproduktion. Um einen guten Betrieb dieses Systems zu gewährleisten, ist eine kontinuierliche Überwachung der Arbeitsbedingungen unerlässlich, um ein akzeptables Produktivitätsniveau aufrechtzuerhalten. Das wertvollste Werkzeug zur Analyse der Leistung des Gestängetiefpumpen ist die Dynamometerkarte. Die Interpretation solcher Karten ist jedoch zeitaufwändig und erfordert das Wissen eines erfahrenen Experten. Ein neuer Trend kam hinzu und löste das Problem der Abhängigkeit von Zeit und menschlichem Fachwissen. Bei diesem Trend handelt es sich beispielsweise um Künstliche Neuronale Netze (ANN).

In dieser Arbeit werden zwei Arten von ANN verwendet, die erste ist das Back Propagation Neural Network (BPNN), der als traditionell betrachtet wird, da es vor dem Einsatz zum Extrahieren von Merkmalen eine Merkmalsextraktion erfordert, und der zweite ist das Convolutional Neural Network (CNN), das Bilddaten direkt verwenden kann, ohne sie vor dem Training zu verarbeiten. Beide Netzwerke verwenden 6132 Dynamometerkarten, die für BPNN wie folgt verarbeitet werden müssen; Jede Dynamometer-Karte, die durch eine in einem PNG-Format gespeicherte Bilddatei dargestellt wird, wurde als ein Satz von (x, y) - Werten vorbereitet, die dann in einen Satz elliptischer Fourier-Deskriptoren umgewandelt werden, die die gesamte Karte vollständig beschreiben. Nach der Datenaufbereitung wurden die beiden Klassifizierungsmodelle für das maschinelle Lernen erstellt, mit Präzision und Rückruf sowie mit einer Verwirrungsmatrix und einem F1-Score bewertet und durch Kreuzvalidierung getestet.

Die vorgeschlagenen Modelle werden unter Verwendung von Daten der realen Felddynamometerkarten trainiert und getestet. Etwa 30% dieser Karten stehen für einen normalen Pumpzustand der Gestängetiefpumpen und 70% für Funktionsstörungen. Die Daten enthalten insgesamt fünf verschiedene Pumpenzustände, Pumpe aus, Gasinterferenz, Leckage des Fahrventils, Auftreffen der Pumpe oben und normaler Pumpenzustand. Für das Training wurde der Datensatz in verschiedene Untersätze aufgeteilt, 80% der Daten wurden für das Training und 20% für das Testen verwendet. Sowohl das CNN als auch das BPNN lieferten sehr gute Ergebnisse.

Diese Studie ist ein ursprünglicher Beitrag zu den automatischen Untersuchungen der Dynamometerkarten und der genauen und schnellen Erkennung von Ausfällen der Gestängetiefpumpen.

Abstract

Sucker rod pumping is the most frequently used artificial lift method for boosting oil production. To insure a good operation of this system, a continuous monitoring of its working conditions is essential to maintain acceptable productivity levels. The most valuable tool for analyzing the rod pumping system performance is the dynamometer card. However, the interpretation of such cards is time consuming and requires the knowledge of an experienced person. A new trend came along and solved the problem of time and human expertise dependency. This trend is in instance artificial neural networks (ANN).

In this work two types of ANN are used, the first one is the back propagation neural network (BPNN) which is considered traditional as it requires feature extraction from the data before using it for data learning and the second one is the convolutional neural network (CNN) which is able to use image data directly without processing it prior to training. Both networks use 6132 dynamometer cards which for BPNN requires processing as follows; each dynamometer card, which is represented by an image file stored in a PNG format, was prepared as a set of (x,y) values which are then converted into a set of Elliptic Fourier Descriptors which fully describe the whole card. After performing the data preparation, the two machine learning classification models were created, evaluated using precision and recall as well as confusion matrix and F1-score and tested by use of cross validation.

The proposed models are trained and tested by using real field dynamometer cards data. About 30% of these cards represent normal sucker rod pumping condition and 70% represent malfunctions. The data contain in total five different pump states, pump off, gas interference, travelling valve leak, pump hitting on top and normal pump condition. For training the dataset was separated into different sub-sets, 80% of the data were used for training and 20% for testing. The CNN as well as the BPNN produced very good results.

This study is an original contribution to the automatically investigations of the dynamometer cards and the accurate and quick recognition of the rod pumping systems failures.

Table of Content

	Page
1 INTRODUCTION.....	1
2 SUCKER ROD PUMP SYSTEM FUNDAMENTALS	2
2.1 Working principle	2
2.2 Sucker rod pump structure.....	3
2.2.1 Surface components	4
2.2.2 Subsurface pump.....	5
2.2.3 Sucker rod string.....	5
2.3 Sucker rod pump monitoring.....	6
2.3.1 Dynamometers	6
2.3.2 Fluid level monitoring	7
2.3.3 Production testing	7
2.3.4 Pump valves condition check.....	8
2.4 Sucker rod pump failures	9
2.4.1 Sucker rod pump vulnerabilities	9
2.4.2 Failures analysis	10
2.4.2.1 Fault tree analysis definition.....	10
2.4.2.2 Fault tree failure analysis representation.....	10
2.4.3 Failures detection	13
2.4.3.1 Dynamometer cards.....	13
2.4.3.2 Fluid level monitoring	16
3 SUCKER ROD PUMP SYSTEM SURVEILLANCE	17
3.1 Group1: sensing function	17
3.1.1 Rod Load measurement	17
3.1.2 Rod position measurement	19
3.2 Group2: Pump off controller.....	20
3.3 Group3: Operational Control.....	22
3.3.1 Remote Terminal Unit (RTU)	22
3.3.2 Master Terminal Unit (MTU).....	23
3.3.3 Communication Channels.....	23
3.4 Integration of reservoir and facilities constraints	23
3.5 Sucker Rod Pump Optimization	25
3.5.1 Sucker rod pump best practices.....	25
3.5.2 Variable Speed Drive	27

4	SUCKER ROD PUMP FAILURE ANALYSIS WITH MACHINE LEARNING	29
4.1	Motivation	29
4.2	Objective	29
5	PROCEDURE	30
6	IMPLEMENTATION OF THE PROCEDURE	31
6.1	Data Assembly	31
6.2	Feature extraction	32
6.2.1	Dynamometer cards contour coordinates extraction	32
6.2.2	Elliptical Fourier Descriptors implementation	33
6.2.3	Fourier Descriptors Application	35
6.3	Model Construction	36
6.3.1	Back propagation neural network	37
6.3.1.1	Back propagation neural network Principle	37
6.3.1.2	Back propagation neural network construction	39
6.3.2	Convolutional neural network	40
6.3.2.1	Convolutional Neural Network Principle	40
6.3.2.2	Convolutional Neural Network Construction	42
6.4	Model Evaluation	43
6.4.1	Confusion matrix	43
6.4.2	Precision, recall and F1 score	45
6.5	Model Validation and Selection	47
6.5.1	K-Fold Cross-Validation	47
6.5.2	Model Selection	49
6.6	Model testing	50
6.6.1	Back Propagation neural network testing	50
6.6.2	Convolutional neural network testing	51
7	RESULTS AND DISCUSSION	52
7.1	Results	52
7.1.1	Back Propagation Neural Network results	52
7.1.2	Convolutional Neural Network results	53
7.2	Discussion	54
7.2.1	BPNN and CNN comparison	54
7.2.2	Recommendations	55
	CONCLUSION	56
	LIST OF TABLES	57

LIST OF FIGURES	58
ABBREVIATIONS	60
REFERENCES	61

1 Introduction

Artificial lift techniques are widely applied in oil industry to improve a well production performance. Although there are several artificial lift methods in the industry (such as Gas Lift, Electric Submersible Pump, Progressive Cavity Pump and Sucker Rod Pumps), The most commonly applied artificial lift technique is the sucker rod pump system with approximately 85% of the lifted wells worldwide. Figure1 shows this fact.

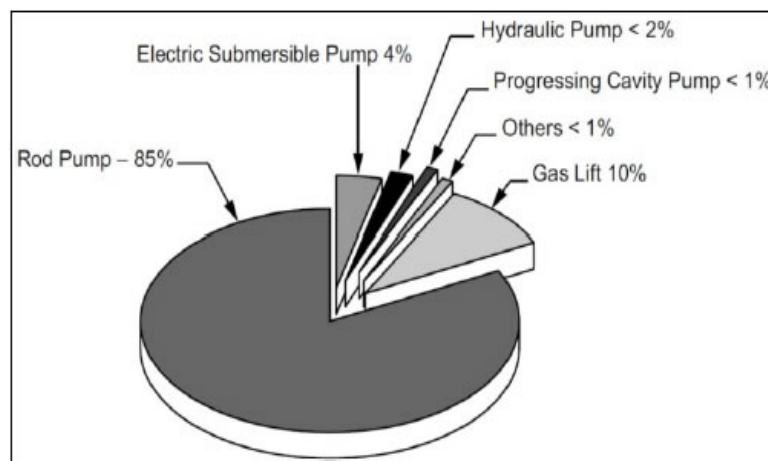


Figure 1: Usage of Artificial Lift Systems Worldwide [18]

Sucker rod pump failures can drastically reduce a well production capacity and can significantly increase the lifting costs. Hence, as soon as an anomaly is detected, proactive repair actions have to be scheduled as soon as possible to improve the system efficiency. The most popular evaluation tool used in the oil industry for the sucker rod pump system is the downhole dynamometer card which is a closed plot that displays the polished rod load versus the plunger displacement. The diagnosis of the system condition is done by interpreting the shape of the pump card. For example, when the pump is functioning properly, the card will have a rectangular shape and when a failure takes place, the pump card takes another representative shape. However, a continuous visualization of the pump card by an expert is both time consuming and prone to human mistakes. The pump card can be analyzed automatically by digital image classification. Recently, artificial intelligence technologies have been involved extensively in the automation of remote sensing applications. ANN (Artificial neural network) technology is applied widely in the classification process of remotely sensed image data. By the application of this approach, the system performance can be significantly improved by adjusting its operating parameters in the right time or by scheduling an early maintenance to reduce downtime. (Marco A. D. Bezerra, Leizer Schnitman, M. de A. Barreto Filho 2009)

The aim of this work is to investigate a set of five anomaly classes by analyzing their corresponding dynamometer cards, using two different types of Artificial Neural Networks, the first one is called the back propagation neural network (BPNN) and the second one is called the convolutional neural network (CNN).

2 Sucker Rod pump System Fundamentals

At oil well early stages, the well is flowing naturally without any external support and the well is called a flowing well. (Numerical simulation of the sucker-rod pumping system 2014) However, after certain time, the reservoir drive energy is diminished at a point that the well is not able to lift fluids to the surface. At this point, an external support must be introduced to compensate for the well production losses, and it can be particularly an artificial lift method. One of these methods is a sucker rod pumping system. The history of sucker rod pump started with the use of wooden walking beams with a cable tool that lift and drop the drilling bit to drill wells. When a well stops to flow naturally, revitalizing it was quite simple; the previous drilling unit is slightly modified, and the drilling bit is replaced by a plunger. This lifting unit was driven by steam power. The wooden walking beam, cable tool and plunger combination launched the sucker rod pump history. Nowadays, sucker rod pumps work based on the same previous principle but does not rely on wooden walking beam and steam power Analyzing this system primarily requires an understanding of its working principle, its components, affecting parameters, vulnerabilities and its monitoring techniques. (Takács 2003)

2.1 Working principle

The sucker rod pump working principle is described by a pumping cycle that has two strokes, the upward stroke and the downward stroke, which are illustrated by Figure 2.

At the beginning of the upward stroke and after the plunger has reached its lowermost position (Bottom Dead Center), the travelling valve closes by the high fluid hydrostatic pressure in the tubing above it. At the same time, the barrel pressure drops, and it is exceeded by the pump intake pressure, as a result the standing valve opens. Fluid from the formation flows into the barrel through it and at the same time fluid in the tubing above the travelling valve is lifted to the surface. This continues until the end of the upward stroke. During this stroke, the full weight of the liquid column in the tubing string is carried by the plunger and rod string connected to it. (Takács 2003)

By the start of the downward stroke, the plunger is at its uppermost position (Top Dead Center). The travelling valve is closed, and the standing valve closes when formation fluid stops flowing to the barrel by the influence of the fluid column weight. When the plunger moves downward and emerges into the fluid inside the barrel, the travelling valve opens, and the liquid weight is transferred from the plunger to the standing valve. At the end of the upstroke, the rod string movement direction is reversed, and another pumping cycle begins. (Takács 2003)

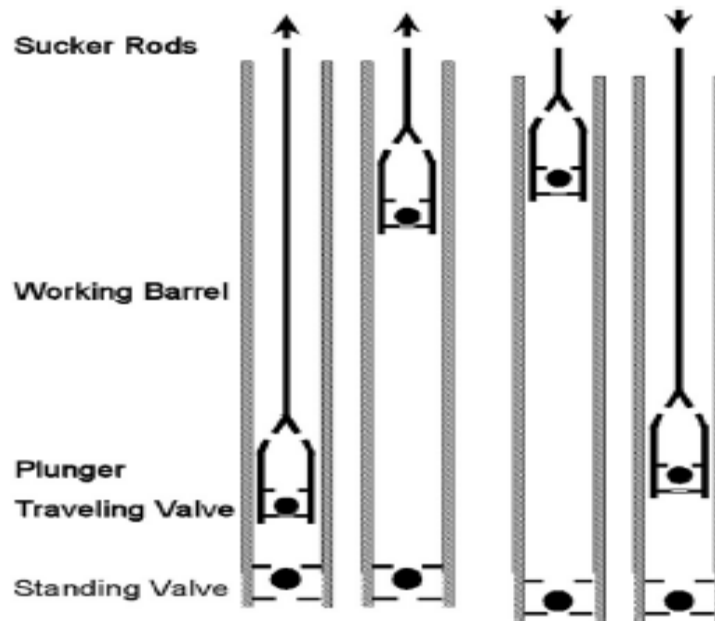


Figure 2: Sucker rod pump working principle [26, p. 62]

2.2 Sucker rod pump structure

A typical conventional sucker rod pump structure is shown in Figure 3. The system can be divided into three main sections: the surface components, the downhole pump components, and the sucker rod string.

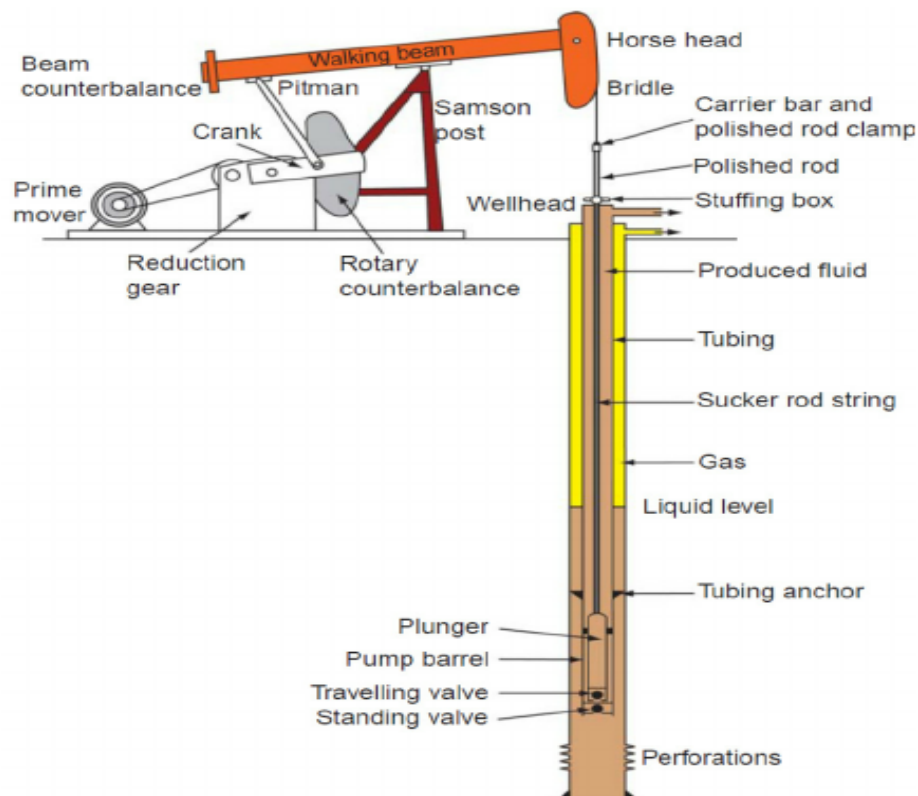


Figure 3: Sucker rod pump system structure [18]

2.2.1 Surface components

The elementary surface components of a sucker rod pump are the prime mover, the gearbox, the pumping unit and the wellhead assembly. (Rod pumping overview 2018)

1. Prime mover

The prime mover provides the driving power to the system and it can be an electric motor or an internal combustion engine which is generally a gas engine. If there is gas available, it is more convenient to use a gas engine although the investment cost of such an engine is higher than that of an electric motor since electricity costs are constantly increasing. However, most sucker rod pumps are driven by an electric motor with three phase power supply (460 volts and 60 Hz), this popularity of electric motors is due to their relatively moderate cost with easy monitoring and control as well as their flexibility for automatic processes.

2. Gear reducer

The gear reducer is an essential component in the pumping unit, and it represents about 50 percent of the pumping unit investment cost. It reduces the high rotational speed of the prime mover to the required pumping speed, and simultaneously, increases the available output torque to fit the required loads.

3. Pumping unit

The pumping unit provides a mechanical link between the gearbox and the downhole pump at the horsehead and transforms the rotary motion of the first part into a reciprocating motion required to move the rod string upward and downward. Its preliminary components are:

- * The horsehead which transmits walking beam forces to the bridle.
- * The walking beam which by means of the equalizer is connected to the pitman and it works on the principle of a mechanical lever.
- * The crank arm which rotates synchronously with the gearbox slow-speed shaft rotation.
- * The pitman which links the crank arm to the walking beam.

4. Wellhead assembly

A typical wellhead assembly consists of:

- * The Polished rod which connects the walking beam to the sucker-rod string, transfer the pumping loads to the surface pumping unit and ensures a sealing surface at the wellhead to keep well fluids in the well. It holds the dynamometer survey as well.
- * The stuffing box which seals on the polished rod.
- * The flowline in which the produced fluid as well as the separated casing-annulus gas are discharged.
- * The pumping tee which directs the produced fluids into the flowline.
- * The check valve which prevent the produced fluid from flowing back from the flowline to the well.

- * The casing vent line which is connected to the flowline and enables the casing-tubing annulus gas to be directed to the flowline.

2.2.2 Subsurface pump

The subsurface pump is mainly composed of a pump barrel, a pump plunger and two working valves. It can be equipped with auxiliary equipment such as valve cages.

1. Pump barrel

A pump barrel is a one-piece hollow tube with threads on both sides. A ball valve, called standing valve, which acts as a suction valve for the pump and through which well fluids enter the pump barrel during upstroke is coupled to it.

2. Pump plunger

A pump plunger is a moving part which is connected to the rod string and houses a ball valve, called travelling valve, which during the upstroke, lifts the liquid contained in the tubing.

3. Pump valves

They are two valves: one travelling valve which opens during downstroke to receive fluid and closes during upstroke to carry fluid to the surface and one standing valve which opens during upstroke to receive fluid formation and closes during downstroke to keep fluid within the barrel.

4. Valve cages

It is an auxiliary equipment to be set on the travelling or standing valve and it controls the lateral and vertical valves movement, meaning that the valve is not capable of moving off its central pathway. As a result, pump valves are prevented from hitting their respective valve seat and a wear both for the ball and seat is prevented.

2.2.3 Sucker rod string

The sucker rod string is the backbone of the sucker rod pumping string, it is the mechanical link between the surface driving equipment and the bottom hole pump. It is mainly composed of individual sucker rods and rod joints. It may be also equipped with auxiliary components such as rod guides and sinker bars. (Takács 2015)

1. Sucker rods

They are individual rods that are connected to each other until the pumping depth is reached. Rods could be made of steel or fiberglass. The major types of steel rods are continuous rods; hollow rods, rod tubes or flexible rods. In general, steel rods have some disadvantage such as a heavy weight which increases the surface power requirements and limits the pumping depth; steel rods are also susceptible to corrosion. That is why they are normally heat-treated during manufacturing to increase their corrosion resistance. However, Fiberglass rods overcome the previous disadvantages since they have much lighter weight which will decrease the energy costs and may demand of a smaller pumping unit.

They have also an inherently high corrosion resistance which reduces the workover costs. However, fiberglass rods have some drawbacks such as the temperature limitations, the low mechanical damage resistance and the high investment cost compared to steel rods.

2. Rod joints

They are connections that ensure the rod string integrity. They are mainly composed of pins and couplings which are prone to material fatigue caused by load fluctuations during pumping operation. This demand a proper rod makeup to insure a high resistant joint against repeated loading and unloading

3. Rod guides

They are small equipment attached to the rod string in different positions and they have many benefits; they centralize the rod string which decreases the material fatigue and prevent the friction, wear and rod-tubing contact. It can also be used with rod rotators to clean the tubing from paraffin accumulation. Rod guides are normally made of strong plastic materials which make it a corrosion resistant.

4. Sinker bars

They are simply heavy sections of steel rods that are connected both to the rod string lower section and the upper bottomhole pump extremity. Their function is to increase the rod load which boosts the pumping rate. They are also used to prevent the rod lower part bucking during the downstroke as well as eliminating excessive compressive loads on the rod string.

2.3 Sucker rod pump monitoring

The most common and valuable tool to assess the sucker rod pump performance is analyzing dynamometer cards. In addition, well testing is used to evaluate the well inflow performance, echo-meters are addressed to find the annular casing-tubing fluid level by means of acoustic waves and pump valves check test is used to ensure proper pumping operation.

2.3.1 Dynamometers

The dynamometer is an instrument that records rod loads versus the rod displacement or the pumping time and results in a closed load-travel diagram. Since the loads registered by the dynamometer represents the pumping system overall acting forces, this is a valuable mean to evaluate the downhole pump as well as the surface pumping unit operation. Therefore, it is possible to detect and analyse the different pumping system failures which allow for production optimization and decision on a workover necessity, it is also possible to assess the prime mover energy requirements and reduce the overall lifting costs, it also allows for the pumping unit adjustment in terms of counterbalance. Dynamometer surveys can mainly be classified into surface dynamometers and downhole dynamometers. (Takács 2015)

2.3.2 Fluid level monitoring

The most common method to locate the casing tubing fluid level is the echo meter or echo sounder. It sends an acoustic pressure wave that travels down along the tubing casing annulus column to the Fluid Level by generating an Acoustic Pressure Pulse that travels down the well, reflects off every depth where it encounters a cross sectional change caused by tubing collars, well fluids, casing liners, perforations,....., The reflected sound waves are picked up, recorded and converted to electrical signals by an internal microphone inside the fluid gun recorded on a paper or by electronic means. The plot of the acoustic reflection is called the acoustic trace as showed in figure 3. An evaluation of the reflected signals reveals the fluid level inside the tubing casing annulus. The further time taken by the wave to be reflected to the surface, the deeper the fluid level is. The determination of the fluid level is as follows: either by counting the collar signals above the fluid level and then related to the well records or by means of both reflection time and wave acoustic velocity as **eq.1** [27, p. 472] states:

$$L = \frac{\Delta t v_s}{2} \quad (1)$$

Where: Δt is the wave reflection time in s, v_s is the wave acoustic velocity in ft/s and L is the fluid level in ft.

Determining the fluid level in the tubing casing annulus; other than assessing the well performance, it allows for the quantification of the amount of pumpable liquid above the pump and the bottomhole pressure. Figure 4 presents an example of a fluid level trace as showed in echo meter's software. Every local peak reflects tubing colors, casing colors, perforations... The red "C" line represents the last collar depth and eventually the "LL" line which is situated just before the triangle shape display indicates the fluid level within the casing-tubing annulus. (Downhole Diagnostics 2018)

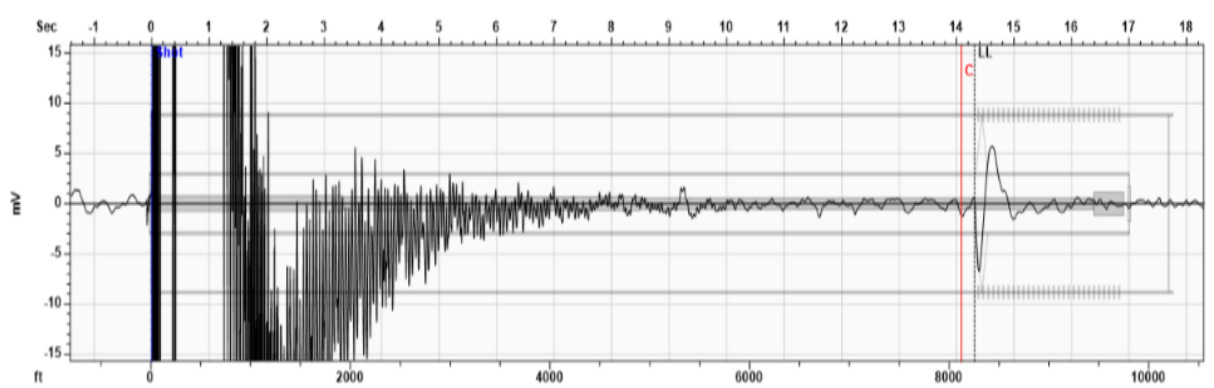


Figure 4: An echo-meter fluid level trace [6]

2.3.3 Production testing

Sucker rod pump production rates calculation is crucial for the well inflow performance behavior analysis. This is accomplished directly either by liquid rates measurements with gauges in tanks or using lease automatic custody transfer (LACT) or indirectly using the downhole pump card which delivers the plunger effective stroke length.

As **eq2** [27, p. 472] states, multiplying the plunger effective stroke length by the plunger cross sectional area will deliver the produced fluid volume during one pumping cycle. (Takács 2015)

$$\Delta V = A_p S_{ef} \quad (2)$$

Where: ΔV is a one pumping cycle fluid volume, A_p is the plunger cross sectional area and S_{ef} is the plunger effective stroke length. Any stroke length loss for example due to tubing stretch or pump leakage must be considered in the effective stroke length determination.

2.3.4 Pump valves condition check

Proper sucker rod pump operation is directly affected by the condition of the standing and the traveling valves. Both valves operation depends on a proper seal between their seats and balls. However, due to mechanical damage, corrosion, or other operational problems, a valve ball and seat seal can be easily damaged. Therefore, it is crucial to frequently check the condition of the pump valves by means of a dynamometer.

The standing valve test

The standing valve test is used to check the standing valve condition for leaks, and it is performed with a dynamometer which is placed on the polished rod. First, the pumping unit is stopped during a pumping cycle downstroke (at about three-quarters of the way down). At this point, the dynamometer measures the actual polished rod load while the standing valve is closed, and the traveling valve is open. Since liquid load is fully carried by the standing valve, the recorded polished rod load represents the buoyant weight of the rod string only. If the standing valve has no anomalies, the polished rod load remains steady when repeating the record and in case the standing valve is leaking, pressure below the traveling valve will be progressively reduced and slowly the travelling valve will close. A part of the load which was initially carried by the standing valve is transferred to the travelling valve which will lead to an increase in the polished rod load. The rate of load increase shows the severity of the standing valve leak condition. (Takács 2015)

The traveling valve test

The TV test is done with the same arrangement as the standing valve test but with a pumping unit stopped on the upstroke (near the top of the stroke). When the pumping unit is stopped, the dynamometer records the polished rod load while the traveling valve is closed, and the standing valve is open. The recorded polished rod load represents the sum of the rod string weight in well fluids and the fluid load acting on the plunger. The standing valve is open and carries no load. If the traveling valve is working properly, then the polished rod load will not change with time and if it is leaking, the pressure between the two valves will increase progressively and the standing valve will close eventually. Fluid load which was carried by the plunger and the rod string will be transferred to the standing valve and the tubing. This is deduced when the new polished rod load is always higher than the load measured later. The rate of load decrease is an indication of the traveling valve leaking severity. (Takács 2015)

2.4 Sucker rod pump failures

Any equipment failure is defined as an undesired event in which the equipment performance is not meeting the target expectation any longer. In other words, an equipment fails when it becomes unable to perform its intended task or function properly or when it stops completely working. A failure can be caused by a single sudden event or by a progressive event or by a combination of dependent events. For the case of sucker rod pump, failures can happen easily progressively and seamlessly, and the consequences are tough which in worst cases demand a workover rig for downhole equipment servicing which is time and cost consuming. That is why failure analysis and detection are the first step to work on failures prevention. Before digging into analyzing the different failures that can affect a rod pumping system, it is convenient to point out our system vulnerabilities.

2.4.1 Sucker rod pump vulnerabilities

Despite its wide range of applications, its relatively high efficiency (50 to 75 percent) and its constant development, the sucker rod pump system suffers from several limitations (Takács 2003), the most important ones are as follows:

- * Operating pumping depth which cannot exceed 16.000 ft, due to the limited mechanical strength of the rod string because of the high weight of the steel rods.
- * Maximum operating pumping capacity which is 6000 bpd.
- * Deviated wells present a problem as well since friction of metal parts can create mechanical damage both for tubing and rod string.
- * Free gas at pump intake is detrimental to the pump production capacity and reduces the pump volumetric efficiency.
- * Corrosion which is generated by the contact of the steel material and the produced fluids that might contain chloride, sulfide, oxygen... dissolved in it, and this is destructive to the material and may lead to mechanical damage.
- * Sand and abrasive particles carried with the formation fluid stream which causes a rapid abrasive wear of the barrel, plunger and valves.
- * Paraffin deposition which restricts the well production and difficult to be removed.

2.4.2 Failures analysis

Diagnosing the sucker rod pump failure ontology need to be precise and accurate and requires including all contributors to a given failure. To do so, it is convenient to construct a so-called fault tree which is a diagram that illustrate the relationship among different failures with its corresponding causes and which might include several levels, meaning that the previously mentioned contributors can be on their turn the consequence other contributors.

2.4.2.1 Fault tree analysis definition

Fault tree analysis is a deductive procedure which analyses an undesired event and causes contributors using a top-down workflow and Boolean logic to evaluate a failure history and to understand a system failure hierarchy. The main purpose of the fault tree analysis is to identify failure contributors before the failure occurrence. The construction of the fault tree results in a logic diagram that shows all the possible contributors to an undesired event. The major undesired event is at the top. In our case, it is the sucker rod pump failures which are divided into four major categories. The logical analysis is backward from top to below. Each input event has an output event which by itself can be an input that generates further output events. The logic process continues until the generated output event is an independent or undeveloped event that has no contributors, or its causes are not yet recognized. (Wikipedia 2019b)

2.4.2.2 Fault tree failure analysis representation

Sucker rod pump failures are mainly divided into four groups: pumping unit failures, sucker rod string failure, tubing failure and the subsurface pump failure. It is convenient to construct their four representative fault trees. (ZHANYU GE 1998)

* **Pumping unit failure**

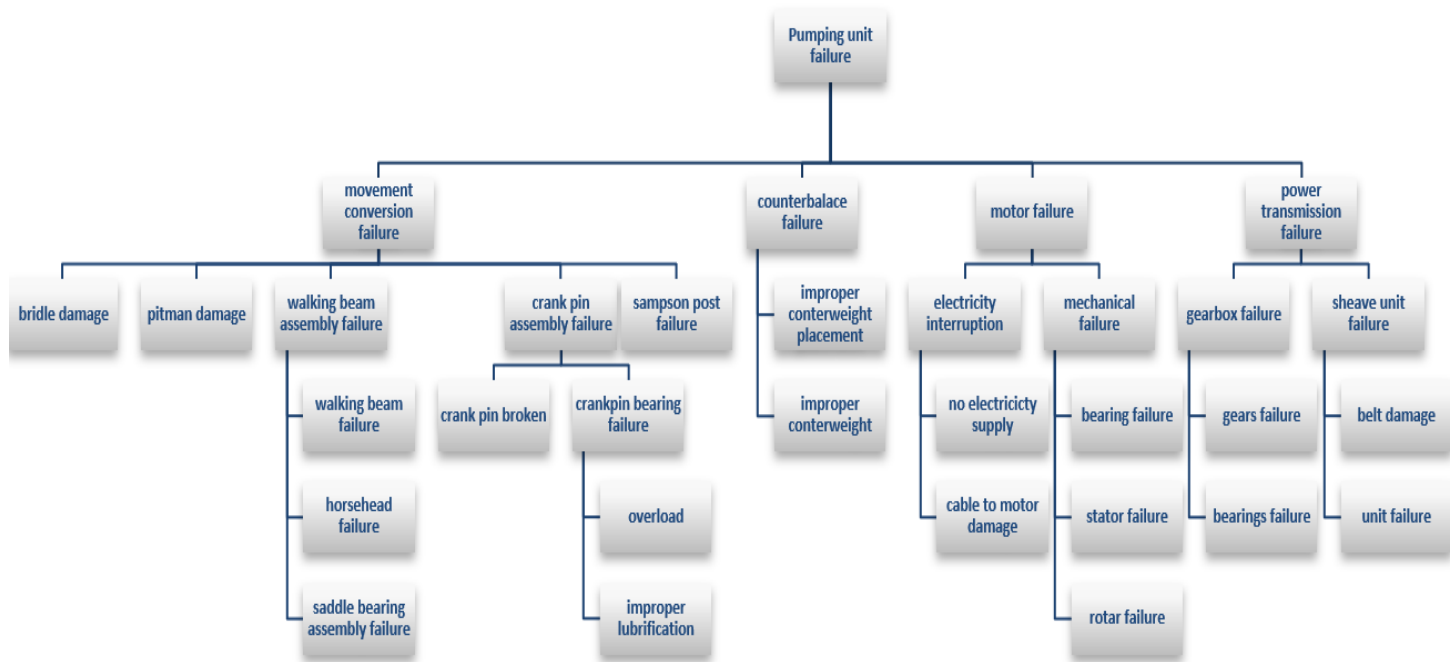


Figure 5: Sucker rod pumping unit failure fault tree representation [34, p. 111]

* **Tubing failure**

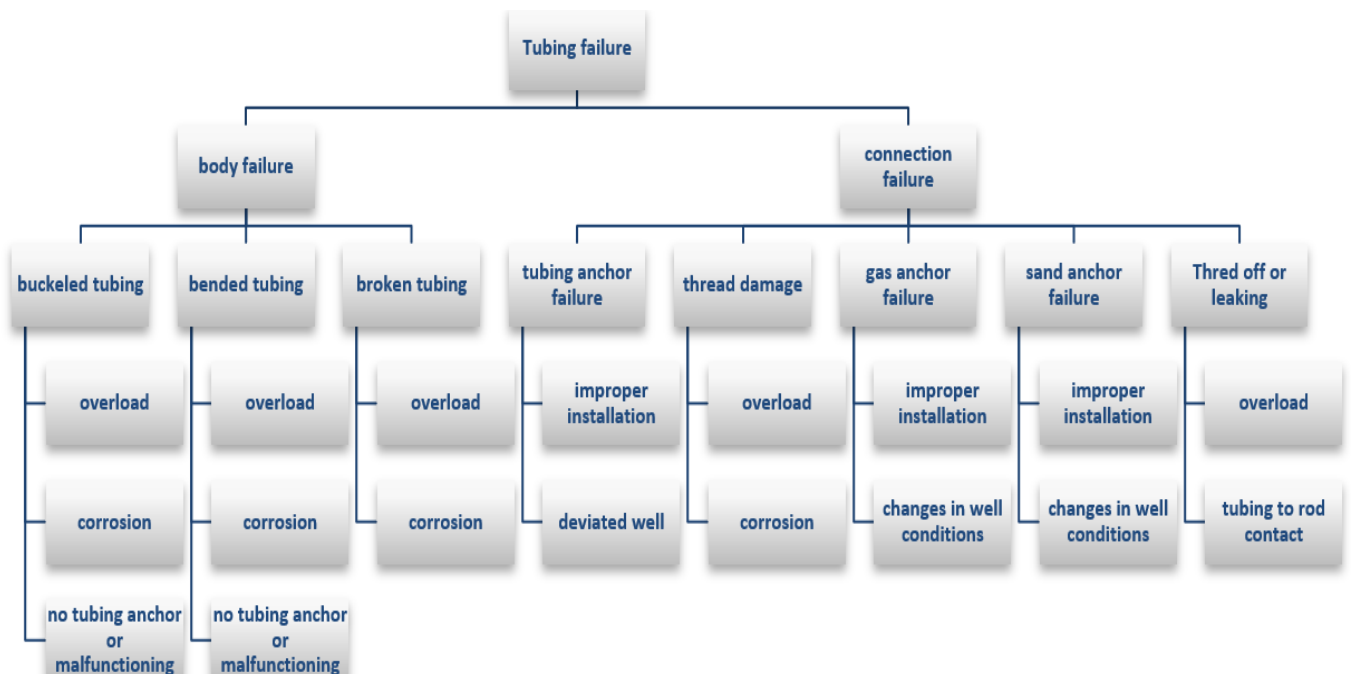


Figure 6: Sucker rod pump tubing failures fault tree representation [34, p. 112]

* **Rod string failure**

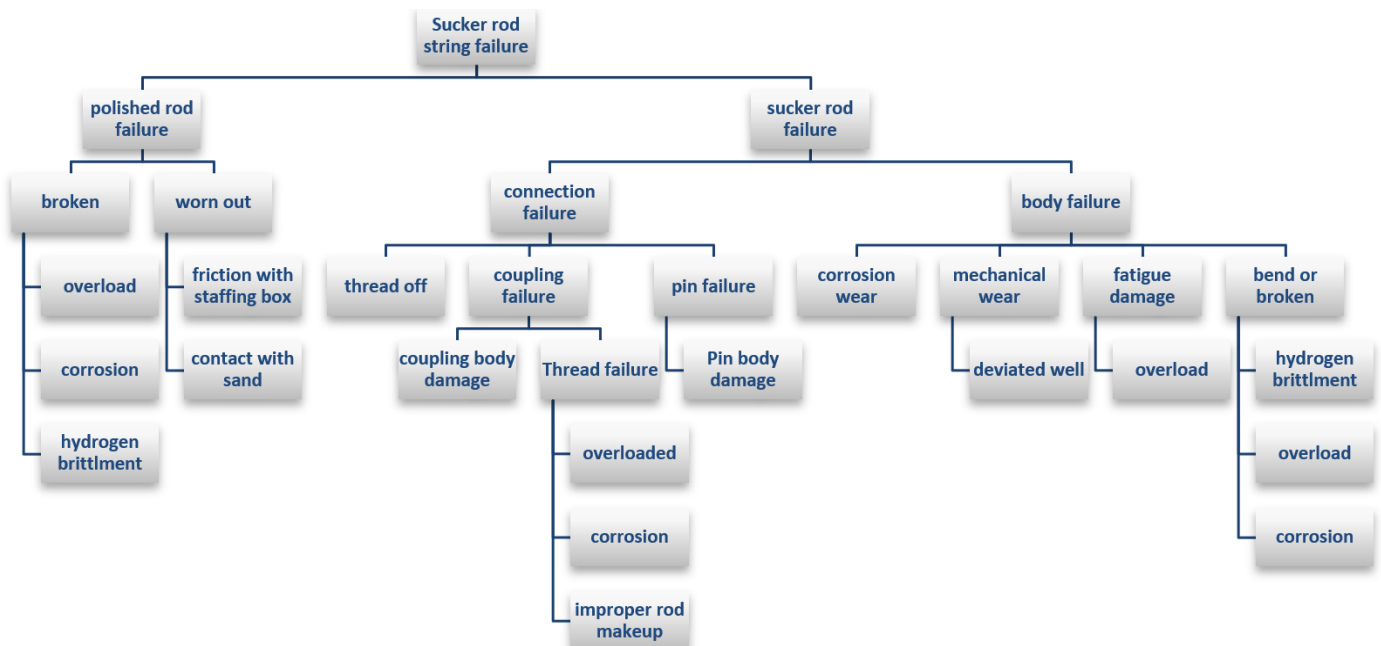


Figure 7: Sucker rod pump rod string failures fault tree representation [34, p. 113]

* **Subsurface pump failure**

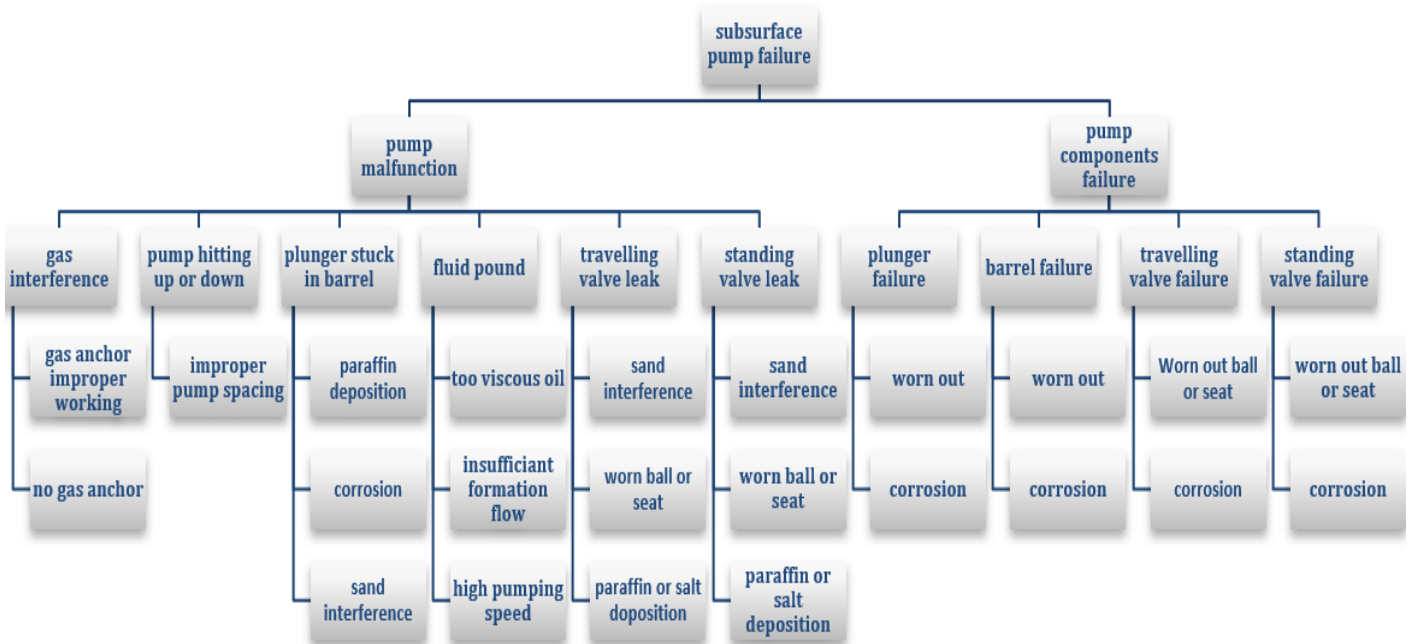


Figure 8: Sucker rod subsurface pump failures fault tree representation [24, p. 114]

2.4.3 Failures detection

The most reliable and widely used method for the sucker rod pump failures detection is the analysis of the dynamometer cards. As many failures are characterized by a typical card shape, it is straightforward to detect a problem if it is correctly reflected on the dynamometer screen. As mentioned before, conventional hydraulic and mechanical dynamometers require the transformation of the pump card from surface to subsurface while electronic dynamometers directly display the subsurface card.

2.4.3.1 Dynamometer cards

Before listing the different dynamometer cards, it is convenient to have an idea how to read such cards. Figure 9 represents a dynamometer card schematic.

* Pump card interpretation

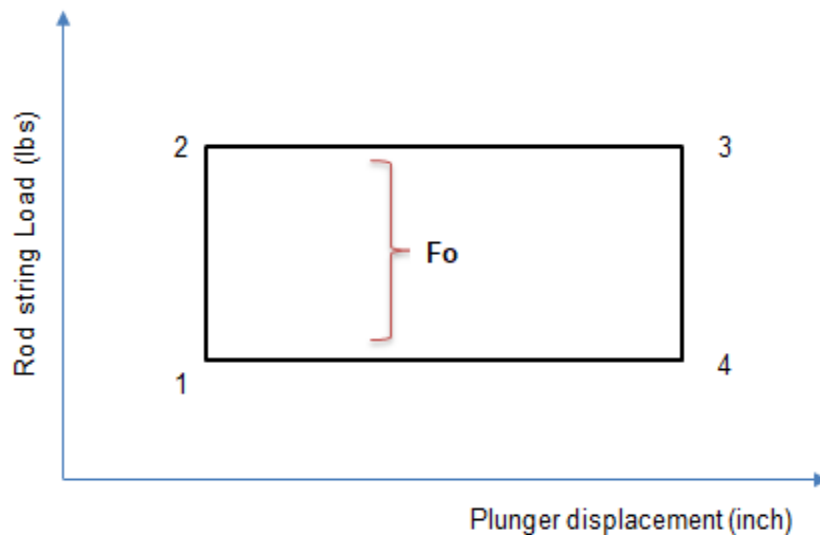









Figure 9: Reference pump card [26, p. 333]






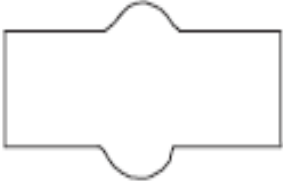


At point 1, the plunger is at the bottom and the two valves are closed. Between 1 and 2, the plunger starts to be lifted by the beginning of the upstroke and take all the fluid load F_0 . At point 2, the standing valve opens to allow the entrance of the formation fluid to the pump. From 2 to 3, the upstroke is still taking place and rods carry the full load F_0 . At point 3, the standing valve closes as the plunger stop going further from the barrel and the downstroke begins. Between 3 and 4, the plunger starts to move downwards and the fluid load F_0 is transferred from the rod string to the tubing. At this point, unanchored tubing will stretch. At 4, the travelling valve opens when the barrel pressure exceeds the pump displacement pressure. From 4 to 1, the barrel fluid is discharged into the plunger until the downstroke is finished and new pumping cycle begins at point 1. (Sucker rod pumping short course 2018)

* Typical Pump cards

The following table displays the major and common dynamometer cards.

Table 1: Typical pump cards [27, p. 489]

Failure	Explanation	Dynamometer card shape
Healthy pump	The pump is working properly.	
Unanchored tubing	The tubing stretches which decreases the stroke length.	
Gas interference	The barrel is filled with both liquid and gas. The pump is partially filled, and the intake pressure gets higher.	
Gas locked pump	The barrel is totally filled with gas. Both valves remain closed and the production stops.	
Fluid pound	The pumping rate is higher than the formation production rate. The Pump is incompletely filled during upstroke.	
Choked pump	The pump intake is plugged and the flow through the SV is zero or less than the plunger displacement.	
Leaking standing valve	This results in a premature loading at the beginning of the upstroke and in a delayed unloading at start of the downstroke.	

Leaking travelling valve	This results in a delayed fluid picking up and in a premature unloading.	
Worn out pump	Both the SV and TV, plunger and barrel are worn out.	
Friction	An excessive friction along the rod string which can be caused by a too viscous fluid and high pumping speed.	
Plunger tagging	The Plunger is hitting on top or bottom. This is due to improper pump spacing or a non-suitable stroke length.	
Sticking plunger	The plunger is stuck at some position along the well and the load spike shows where the plunger has stopped.	
Bent or sticking barrel	The barrel is defected at some position. When the plunger reaches this section on the upstroke, the rod load increases and vice versa on the downstroke.	
Worn or split barrel	The barrel is defected at some point. When the plunger reaches this section on the upstroke, the rod load decreases.	
Delayed TV closing	The TV does not seat when the upstroke begins.	

**Hole in barrel or
plunger pulling
out of the barrel** The load decreases as the
plunger reaches the barrel
hole.



2.4.3.2 Fluid level monitoring

The fluid level monitoring has numerous applications. The most important and common ones are:

1. If the fluid level is low: it means that the intake pressure is low, and the well is pumped off, actions to be taken are dropping the pump seating depth, reducing the SPM, or verifying that the run-time is properly calibrated, so the pump is not pounding fluid.
2. If the fluid-level is high: the pump efficiency is low. It might be time to increase the pumping capacity. Additionally, the high fluid level might be an indication that the corrosion inhibition is not working properly.
3. Fluid level determination also helps in finding casing leaks, whether that knowledge comes from an abnormally high fluid level or a high anomalous up-kick on the Fluid Level Trace (indicating a potential hole). (Downhole Diagnostics 2018)

3 Sucker Rod Pump System Surveillance

Sucker rod pump surveillance is performed by a process control system which allows for remotely tracking the well and equipment parameters that reveal the overall system performance. This process control system is constituted of three functional groups that communicate with each other. The first group performs the sensing activities which are performed by sensors and actuators. For the sucker rod system, the most important sensors are the rod load and the rod position sensor. The second group is mainly the pump off control system and the third group oversees operator control and supervisory control as well as alarming. The core of this group is SCADA system which creates an interface between the control device and the operator.

3.1 Group1: sensing function

As mentioned earlier, rod pump parameters sensing is about measuring the performance relevant parameters of our system such as, the rod load, the rod position, the wellhead and casing pressure and temperature, the fluid flow rate... Only the rod load and the rod position measurements will be described as they are specific to the rod pump system.

3.1.1 Rod Load measurement

The rod load can be measured by a mechanical, hydraulic or electronic dynamometer.

1. Mechanical measuring device

Its essential component is a steel ring which is placed between the carrier bar and the polished rod clamp and which fully support the polished rod load. The resulting ring's deflection is recorded on an attached paper to a rotating drum. Since the rotation of the drum is controlled by the polished rod's vertical movement and the deflection of the steel ring is proportionally related to the polished rod load, the traced record represents the polished rod load against its displacement. The major disadvantage of this device is the need to stop the pumping unit before the steel ring is installed on the polished rod. (Anthony Allison 2015)

2. Hydraulic measuring device

Opposed to the mechanical device, the hydraulic load measuring device can be installed without the need to stop the pumping unit. The dynamometer is composed of two load-sensing hydraulic pistons positioned between the shoulder of the spacer and the carrier bar. First, hydraulic pressure is applied to the pistons. Pistons lift the spacer off the carrier bar and the polished rod load is fully taken by the hydraulic pistons. As a result, the polished rod load variations lead to hydraulic pressure variations, which are recorded by a stylus that magnifies the displacement of a spring-retarded piston. A plot of polished rod load versus polished rod position is recorded on a paper attached to a rotated drum since the rotational angle of the drum is proportional to the polished rod displacement. The major limitation of the hydraulic dynamometer is the accuracy which can be reduced as the measuring spring gets weaker. (Takács 2015)

3. Electronic beam mounted strain gauge

As the name states, the relevant component of this sensor is a beam strain gauge which is placed on the walking beam. It measures changes in the rod load by measuring the changing in the walking beam. A strain gauge is a resistive transducer that converts a mechanical elongation induced by a force into a resistive change. Figure 10 represents an instrumented beam pump and the element E is the strain gauge position in a rod pumping system. A beam mounted strain gauge does not require polished rod to be clamped off during installation or replacement. It also eliminates the risk of cable damage during normal operation or workover. (Anthony Allison 2015)

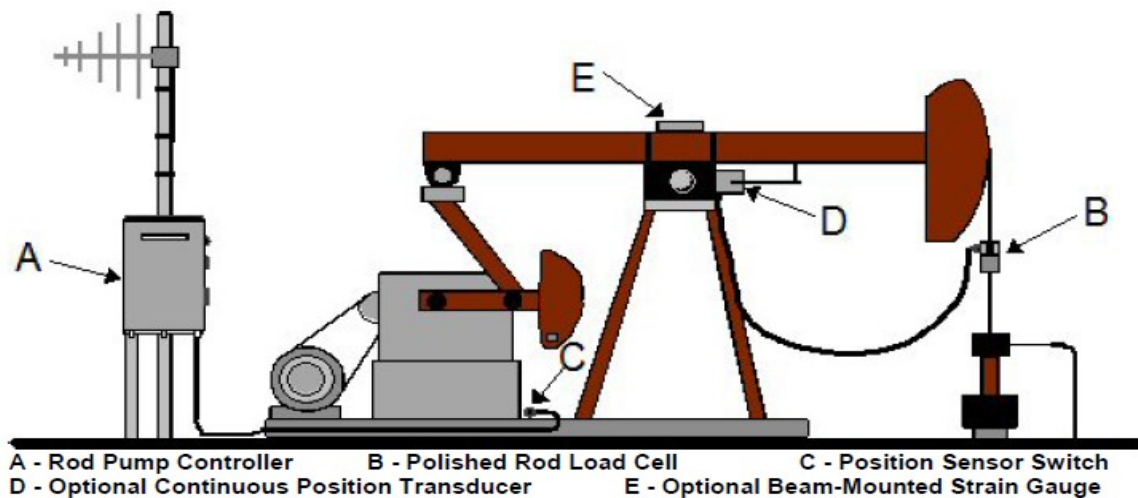


Figure 10: Instrumented sucker rod pumping system [1]

The most important weak point of the beam mounted strain gauges is its poor accuracy which is caused either by a low proportionality between strain gauge output and load on the polished rod or by the additional forces other than the polished rod load which affect the measured strain such as changes in the beam temperature that causes beam expansion and contraction and eventually may leads to errors in the dynamometer card.

4. Electronic Polished rod load cell

As it is clear on Figure 9, the electronic polished rod load cell is Element B and it is installed directly on the polished rod below the carrier bar. it measures the polished rod loads by strain gauges as follows: when radial strain is produced by the polished rod axial loads, it is recorded by the cell and is converted into electric voltage signals which are linearly proportional to the polished rod load. Polished rod load transducers have easy application and the cell sensitivity is almost constant with time. However, major limitation of this sensor is the cable which is susceptible to damage during operation which may lead to measurements errors because of drift of calibration. (Anthony Allison 2015)

3.1.2 Rod position measurement

Devices for position measurements could be a simple position switch, an inclinometer or an accelerometer.

1. Position switch

It is a simple and inexpensive mean to measure polished rod position and as it is illustrated by Figure 11, main components of the device are a reed switch which is embedded in a stainless-steel wand and attached to the pumping unit base and a magnet which is attached to the inside of the crank arm. The working principle is such as when the magnet passes in front of the wand, the switch closes and sends a signal containing a reference position value to the rod pump controller once per stroke through a cable service tool. The top of stroke position must be calibrated to effectively construct the remaining stroke position points. That is why an error may occur when the calibration is not modified after a change in the SPM or in stroke length or in counterbalance. However, even with a good calibration, the position switch will produce low quality position measurements. (Anthony Allison 2015)

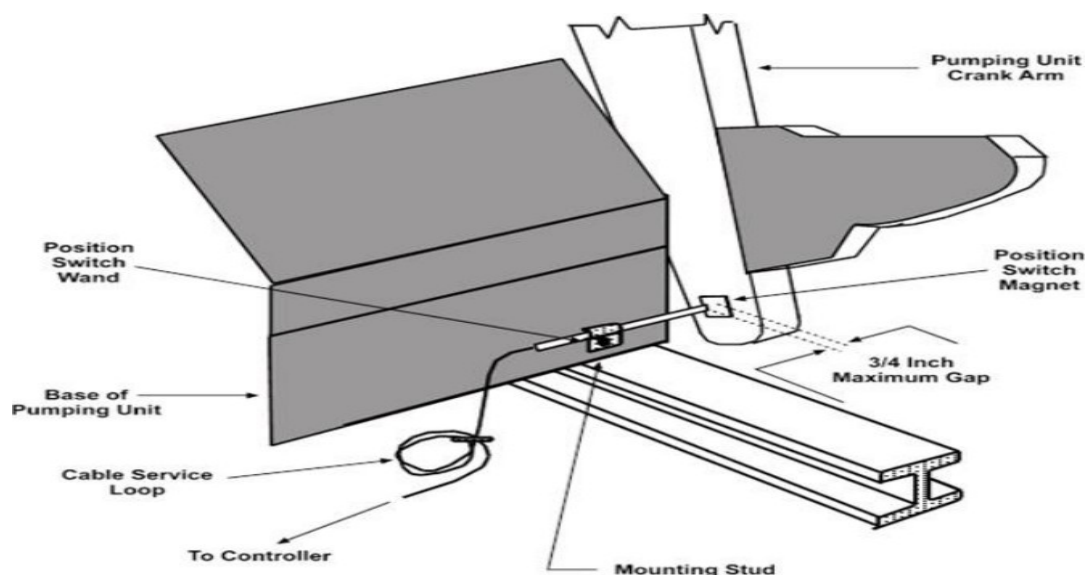


Figure 11: position switch rod load sensor [1]

2. Inclinometer

An inclinometer is shown by Figure 9 as element D. It is a measuring device attached to the walking beam and it is used to measure the angle of the beam as it varies throughout the stroke. It relates changes in beam angle to changes in polished rod position. The sensor installation position is important because a wrong installation will generate a nonrealistic dynamometer card. In fact, a proper installation is on the right side (wellhead to the operator's right when looking at the unit) since it generates an increasing voltage during the upstroke and not the opposite case which will lead to a reversed dynamometer card. (Takács 2015)

3. Accelerometer

An accelerometer is a very small unit permanently attached to the load sensor. It measures the polished rod's instantaneous acceleration accurately. The polished rod position is obtained by integrating the acceleration twice with respect to time. An accelerometer is an accurate and reliable sensor because its resolution is a function of the data sampling frequency and can thus be almost continuous and can instantaneously detect minor changes in polished rod velocity. (Takács 2015)

3.2 Group2: Pump off controller

A sucker rod pump off controller is an intermittent controller which provides an automatic operation as follows: When the pump is operating at a rate more than well inflow, the liquid level in the well drops below the pump intake depth, the pump barrel is partially fill up with fluids during the upstroke. As a result, during the following downstroke, the pump plunger will hit the fluid level in the barrel, what cause the phenomenon of fluid pound and the well is said to be pumped off. At this point, the controller detects the fluid level decrease and shut off the pumping unit for a period until the fluid level rises again in the annulus before restarting the unit. This process is described by Figure 12.

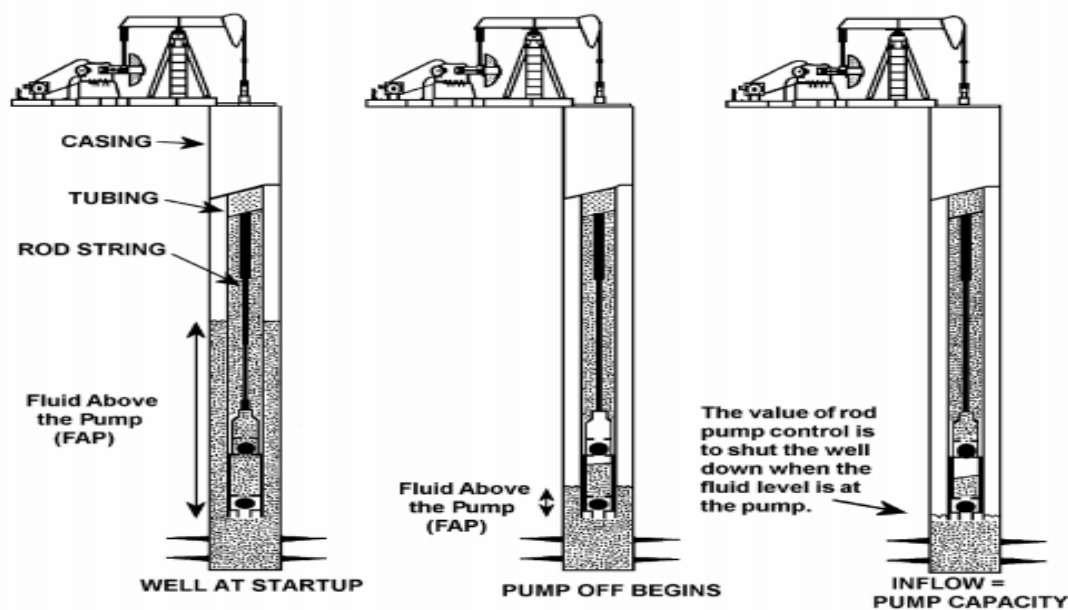


Figure 12: Sucker rod pump off control diagram [33, p. 7]

A pump off controller can be a stand-alone POC which provides local control at the wellhead by periodic on-site adjustments, or it can be connected to a (SCADA) system central computer that receives the collected data and send back control instructions through communications channels. The second type will be explained in the next section. (XIE LU 2014)

A pump off controller can perform different tasks. These include fluid level testing, Flow/No-Flow sensing, vibration detection, and Polished Rod Load and Position sensing.

The fluid level in the tubing casing annulus is detected by means of surface sonic pulses as discussed in section 2.3. The level is automatically monitored such as the pumping unit is

stopped when the level drops to or below the pump intake depth and it restarted when enough fluid has accumulated in the annulus. The vibration detection has a simple mechanical principle that when an important pumping unit vibration is detected, a controlling device stops the prime mover as a vibrating unit means a pump off condition. A flow/ no flow sensor is installed on the flowline. In this case, pump off condition is detected by the decrease in the flowrate along the flowline and the pumping unit is stopped. The previous three systems are considered inaccurate and unreliable compared to the polished rod load and position sensing system. (Takács 2015)

This system relies on the polished rod load and position cells. Both are explained in section 2.1. However, a complete pump off control system requires in addition a control interface to which the load cell and the position cell transmit their sensed data. The control interface after gathering and processing load and position data, it displays the dynamometer card. The control interface is placed at the well location and displays calculated and plotted outputs for the operator through a graphics display. In addition, it allows for the operator to set the pump-off point, a set position and load value at which the well is considered “pumped off.” The operator configures also the number of times the dynamometer card can travel outside the pump-off point before the control interface automatically stops the pumping unit. As well as the down time value once the well pumps off until the unit restarts. In addition to constructing the dynamometer cards, the controller interface stores them for later or real time analysis. When hooked to a field supervisory control and data acquisition system (SCADA) system, the stored large amounts of data, in addition to the sucker rod pump system anomalies detection; it provides a well management and operation control opportunity by the central supervisory computer data analysis. Although the popularity of pump off controllers, this system still has some disadvantages listed above:

- * When the pump is off, the reservoir flow into the wellbore builds a liquid level in the casing, it's the objective of the controller. However, this created backpressure on the producing formation.
- * The repetitive cycle of shutting off the pumping and restarting, requires for each cycle a maximum power usage at the restarting phase and creates a significant shock on the pumping unit as well as on the rod string and the downhole pump.
- * If the well is producing fines or solids, the pumping unit downtime is an opportunity for the solids to settle and this cause the plunger to be stuck.

3.3 Group 3: Operational Control

An operational control of a large process can be achieved only by a supervisory control and a data acquisition (SCADA) system. SCADA system is in fact a critical tool to remotely control, investigate and manage the performance of industrial facilities located at different remote sites. The system is composed of hardware and software. The hardware part which is represented by Figure 13 is composed of a remote terminal unit (RTU) and a master terminal unit (MTU). The RTU collect data from sensors or other data sources and performs a control response with a programmable logic controller (PLC) which can be a microprocessor or a single-board computer. The MTU oversees data analyses and human machine interaction. (XIE LU 2014)

Eventually, RTU and MTU are directly connected via communication channels. The three parts of SCADA system hardware are described individually in the following sub titles. Concerning the software part, it is composed of programs and databases of the MTUs, scripts running on PLCs and graphical user interface (GUI) for human-machine interaction.

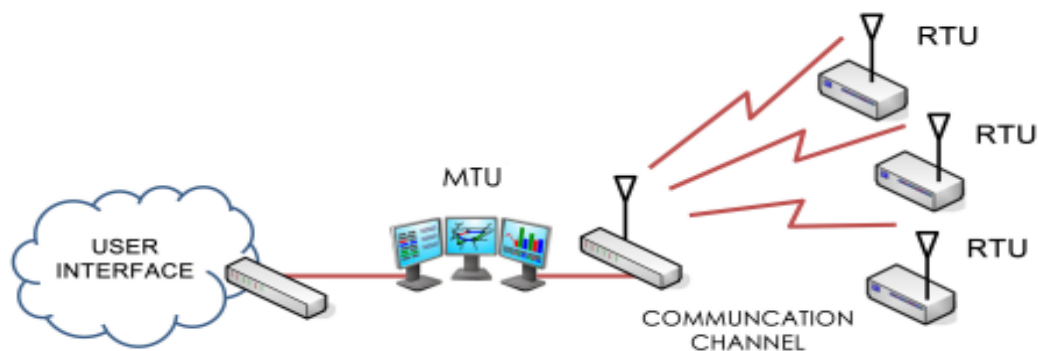


Figure 13: SCADA system architecture [33, p.4]

3.3.1 Remote Terminal Unit (RTU)

As mentioned before, RTU gathers wells operational data at each remote site and transfers it back to MTU via communication channels. It also launches signals to actuators for response control. However, traditional RTUs are not capable of performing calculations. They are like human beings who have eyes, ears and hands, but no heart. That is why; data processing and storage must be done separately on MTUs. This may lead to several issues such as failure of the communication between the RTU and the MTU as well as low feedback control efficiency since it is governed by network speed. These issues are solved nowadays thanks to the rise of programmable logic circuits (PLCs) such as a microprocessor. This improves the communication between RTU and MTU because it is possible to off-load the communication channel and the MTUs by performing calculations locally. Remote terminal units are also known as remote telecontrol units. (ZHANYU GE 1998)

3.3.2 Master Terminal Unit (MTU)

A master terminal unit is an indispensable component of a SCADA system. It is also known as host computer or data server and it is connected to the remote terminal unit via communication channels for data and information exchange. An MTU is responsible for gather data from RTUs, storing data, displaying information and in certain cases it also oversees processing data and giving feedback control signals to RTUs. The communication between the MTU and RTU is bidirectional; however, the key difference between the two components is that the RTU is regarded as a client which provides data required by the server. An MTU normally includes a relational database management system (DBMS) such as SQL-Server or MySQL used for storing a significant amount of field data and supporting a variety of user queries. However, with huge number of sensors generating data continuously, cloud storage and cloud computing might be included into future SCADA systems to provide solutions in the cloud environment. (Master Terminal Units (MTU) in SCADA systems 2011)

3.3.3 Communication Channels

RTUs and MTUs are interconnected via communication channels, which will constrain the speed and security at which data acquisition and control can be performed. These channels typically include copper cables, fiber optic cables, leased circuit, radio links and/or a combination of these techniques. However, after the revolution of WWW, Ethernet TCP/IP has been increasingly used by modern SCADA systems since it overcomes the limitations of analogue communications in terms of continuity and speed of data transfer and provides higher flexibility in terms of expansion and configuration. Developments of wireless sensor networks (WSNs) nowadays make it possible to construct wireless SCADA systems that provide stable and reliable information distribution and long-distance monitoring. Wireless technologies include GSM, GPRS, 3G/4G, WiMAX, Wi-Fi, Bluetooth, ZigBee, and UWB. Many considerations in SCADA system communication channels in terms of security includes access control, firewalls, intrusion detection, key management, as well as operating system security. Optimization of SCADA systems communication channels is possible by upgrading the communication from the RTU-MTU level to RTU-RTU level. (Falah H. Zawahemah 2002)

3.4 Integration of reservoir and facilities constraints

Global operating conditions of the sucker rod pump system need to be performed to insure a complete verification of the system status and to have a clear way to establish an optimization plan. The integrated analysis of the pumping system must include all the following elements: the pumping surface equipment, well downhole components equipment and eventually the reservoir.

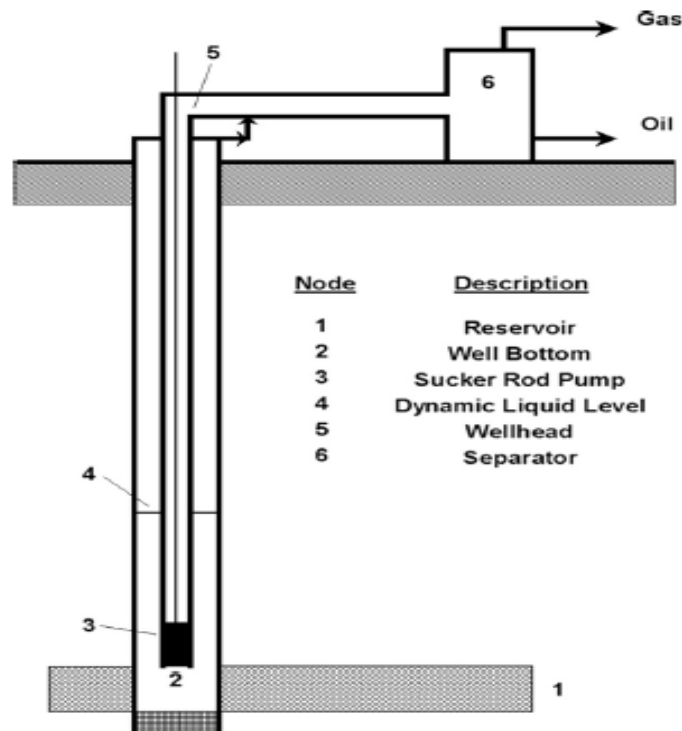


Figure 14: production system of a rod pumped well [27, p. 398]

The mutual analysis of the sucker rod downhole pump, the reservoir and the surface facilities together, is easily performed by a system nodal analysis. This methodology helps to design and study the pump system with a proper consideration for the well inflow performance.

Figure 14 represents a schematic model of a pumping well displaying the different components of the production system separated by nodes. System nodal analysis shows that the reservoir, the well bottom, the sucker rod pump, and the surface facilities including the pumping unit and the wellhead are linked in series. That means that the same flow rate must flow through all components. By considering a two-component system; including the pumping system and the reservoir, an analysis of the reciprocating effect between the two components helps to determine the system effective production rate. On one hand, the pumping system performance is characterized by which is called performance curves, which are constructed by Schmidt and Doty and represents the reachable production rates depending on the pumping conditions (plunger size, stroke length, pumping speed ...) versus the pump setting depth. Performance curves takes into considerations the surface equipment characteristics, the rod string specifications and the overall pump operating mode. On the other hand, the reservoir inflow performance is described by a modified IPR curve which displays the production rate versus the annulus liquid level. By superimposing the two components curves, their intersection points determine the attainable production rates for specific pumping conditions. (Takács 2015)

The method is clarified by Figure 15 which represents an example of a pump performance curve for a system with a C-228D-213-100 pumping unit, a 1,25inch plunger diameter, grade D rods and a rod string with API 86 taper. Horizontal lines display the pumping system performance and each line corresponds to a specific stroke length and pumping speed while the inclined straight line represents the modified IPR reservoir performance with a 3000 ft well depth, a PI of 0,46 bpd/psi and a 1000ft static fluid level. The intersection of both curves delivers the possible achievable production rate with the corresponding pump setting depth.

The maximum attainable flow rate in the example, is 250 bpd with 73-inch stroke length and 4,5 strokes per minutes pumping mode. (Takács 2015)

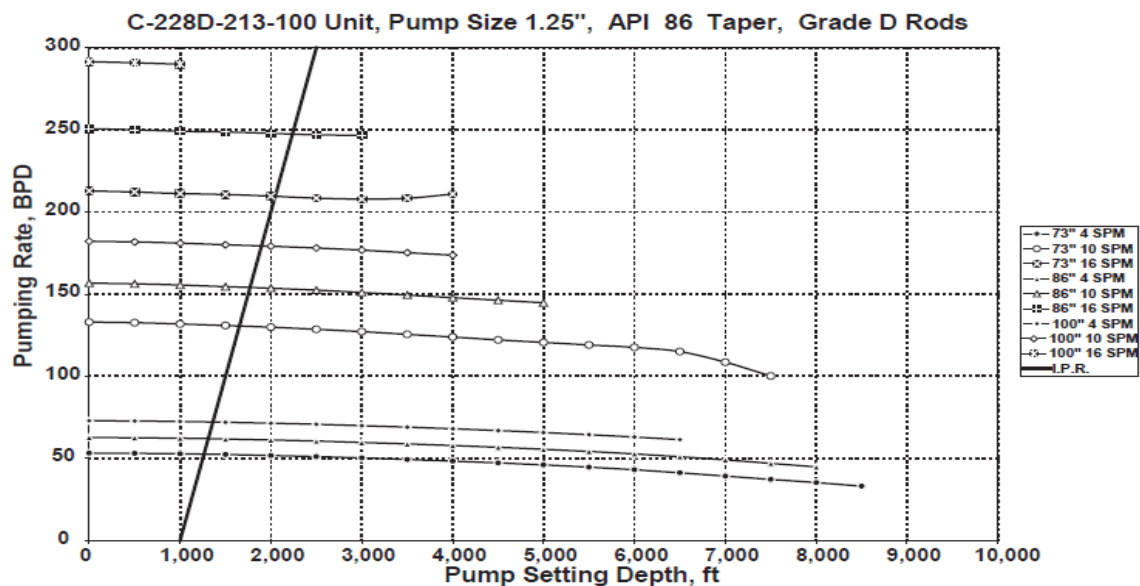


Figure 15: System performance curve sheet for a pumping system with a C 228D-213-100 unit, a 1.25 in plunger, API 86 rod string and Grade D rods [27, p. 403]

3.5 Sucker Rod Pump Optimization

The objective of a sucker rod pump optimization is to maximize the profits from rod pumped wells with minimum pumping costs. To do so, the first step is to design suitably the overall pumping system and operate it effectively then the existing design can be adjusted if some changes promise improvements. In the next section, some good practices to properly operate the beam pump system are listed and justified followed using the variable speed drive in the sucker rod pumping system and its contribution to the optimization.

3.5.1 Sucker rod pump best practices

Good sucker rod pump system practices are listed below in a categorical manner. (Rowlan et al.)

Preliminary practices

- * Size the pumping unit and the prime mover in a way to match the well loads to be lifted.
- * Sustain a good volumetric efficiency via a proper match between the reservoir inflow capacities and the pump production abilities.
- * Continuously check the pump condition by valve checks.
- * Check the well's productivity, the downhole pump performance, the prime mover performance, the downhole gas separator performance and the rod and beam unit loading.

Rod string considerations

- * Rod string design must handle a worst-case scenario: highest SPM, highest loads, highest production rates... because the well conditions changes continuously, and the design must be suitable for all conditions.
- * Integrate rod guides to the rod string which prevent rod/tubing wear and improve rod string and tubing life.
- * Select the rod guides type and material based on the well conditions, for example, gassy wells require nylon guides and high rate and deviated wells require molded on rod guides.
- * The number of rod guides per rod section must be well selected because excessive number may cause significant turbulence and rod stiffness which may cause premature rod failure.

Pump considerations

- * Rod top anchor pumps are suitable for low production and sandy wells and rod bottom anchor pumps are preferred for deep wells.
- * For high volume production wells, casing pump or tubing pump are the best choice.
- * If the pump efficiency is low, the pumping system production capacity must be reduced, and the opposite is true.
- * In case of gas interference, try longer stroke or smaller pump, increase pump intake through higher fluid level, separate gas before entering the pump intake through downhole separation or use a two-stage valve to reduce traveling valve hydrostatic pressure.
- * In case of a deviated well, set the pump below the kick off point for better gas separation.
- * Try to limit the pump leakage to not more than 2-5% of the production.

Gas Separation Best Practice

- * The pump intake should be below the gas entry point into the well.
- * A typical poor boy separator should only be selected for low rates (~50-150 bpd).
- * Properly size the gas separator because an improperly sized separator is worse than no separator as it can trap gas into the pump and as a result the separator becomes gas locked.

Pumping unit considerations

- * Pumping unit loading should be checked by dividing the polished rod load (lbs) by the unit structure rating (100 lbs) and it must be between 40 and 70. If it is lower, the unit is too big for the desired application and this condition will increase power consumption. And if it is higher the unit is too small, and it will not be able to lift the desired fluid rate. (Daryl Curtis 2009)
- * Gearbox loading must be checked by dividing the peak upstroke torque by the gearbox loading and it should be below 85%. If it is higher, the gearbox is likely to be able to withstand the loads and a new unit design must be considered. (Daryl Curtis 2009)

- * Pumping unit must be checked for abnormal sounds, grease or oil leaks.
- * The stuffing boxes tightness must be checked to prevent wear on polish rod and significant output horsepower from motor.

Fluid Level Detection

- * Perform annulus fluid level measurements on a regular scheduled basis.
- * Compare fluid level information with dynamometer cards to confirm if a well is really operating in a pumped off condition.

Casing Pressure

- * Maintain low casing pressure because high casing pressure restricts flow from the formation as a high fluid level does.

3.5.2 Variable Speed Drive

One of the existing opportunities to reduce pumping system energy consumption is the integration of a variable speed drive to the pumping system. A pumping unit is typically driven by an induction motor type AC which is characterized by an electricity frequency dependent speed, and logically the pumping speed is changed by varying the power frequency. Hence, a suitable control of the driving frequency provides that the well pumping rate continuously matches the reservoir inflow since pump displacement is proportional to the pumping speed. Electric frequency is normally regulated by a variable speed drive as follows; the power supply sends an alternating voltage at a constant frequency to the VSD to be rectified to a direct voltage and to be synthesized to produce a current that fluctuates depending on the load on the unit. To perform this function, a typical variable speed drive is composed of a rectifier that converts the AC voltage into a DC voltage, a DC control section that creates a smooth DC waveform, and an inverter that output an AC voltage at a selected frequency. A variable speed drives typically works mutually with the pump-off control system as follows; operational data of one pumping cycle are inputted to the POC which outputs a control signal to the VSD to regulate the pumping speed by altering the received constant frequency power into a variable frequency one fed into the motor. The adjusted pumping speed ensures that the production capacity of the system matches the inflow rate from the reservoir. A typical POC with VSD configuration is represented by Figure 16. The DBR component in the arrangement is a dynamic braking resistor which is responsible for the regenerative power dissipation as heat. Regenerative power is a power that cannot be sent back through the VSD to the power supply and it is created by negative torques which enforces the motor to become an electric generator for portions of the pumping cycle. (Takács 2015)

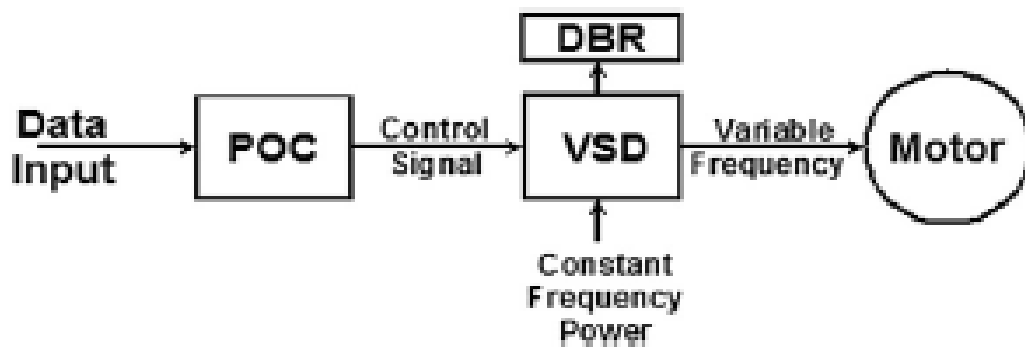


Figure 16: Arrangement of POC and VSD devices for pumping speed control [27, p. 416]

The VSD with the POC perform an automatic operation to maintain a continuous matching of the system's pumping capacity to changing reservoir inflow conditions. This operation is more practically explained by Figure 17 which displays a pump card with a rectangular deadband that represents a reference area to the POC. The operational mechanism is as follows:

- * If pump fillage falls within the set deadband, the VSD unit keeps the pumping speed constant.
- * When the pump fillage values to the left of the deadband, the VSD unit slows down the unit because pump-off condition is approached and the capacity of the pumping system is decreased, consequently, liquid level in the annulus rises and pump fillage increases.
- * When the pump fillage falls to the right of the deadband, the VSD speed up the pumping unit because the reservoir inflow has over increased and the pump capacity must be boosted to match the reservoir inflow and to reduce the liquid level in the annulus.

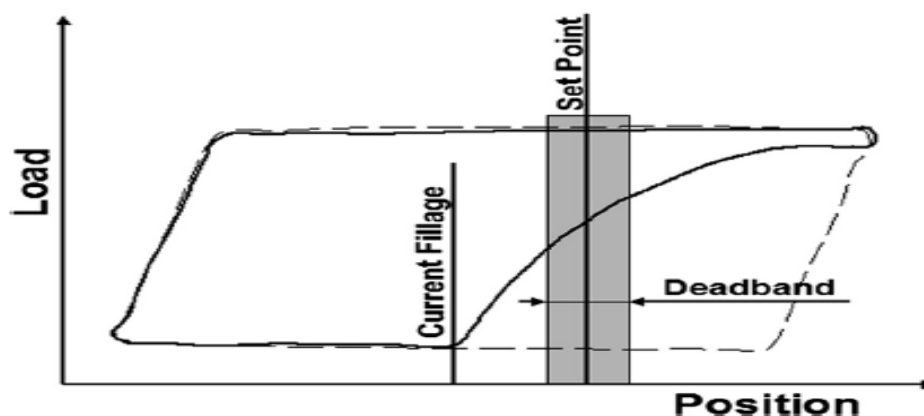


Figure 17: Operational principle of a well manager unit [27, p. 417]

4 Sucker rod pump failure analysis with machine learning

Dynamometer card which is a plot of the sucker rod string load versus the plunger displacement, has become a powerful tool to classify the sucker rod pump system's conditions, since each condition can be characterized by a representative card shape. However, the conventional method to analyze these dynamometer cards by visual interpretation imposes several drawbacks which paved the way to machine learning and particularly to the artificial neural network to be raised and deployed in the automatic analysis of the sucker rod pump dynamometer cards investigations in an effective and quick way. (Corsano 1994) This work is an opportunity to explore artificial neural networks and their use in pump cards analysis by going through its complete deployment cycle from acquiring the cards datasets passing through their preparation and application to build two types of neural networks. The evaluation, validation, selection and testing of the two models will be performed with many techniques in order to assess the performance and effectiveness of machine learning networks in card shapes classification. (Marco A. D. Bezerra, Leizer Schnitman, M. de A. Barreto Filho 2009)

4.1 Motivation

Traditionally, sucker rod pumping failure diagnosis is a process of visually interpreting the pump dynamometer card by experts. However, there are two clear disadvantages related to this conventional method. The first one is that the success of this method is directly dependent on the skill and experience of the analyst and even the most experienced analyst can be misled into an incorrect diagnosis. The other drawback is that this method is time-consuming, which cannot adapt to the modern automatic data acquisition and diagnosis techniques. Moreover, if the dynamometer cards expert is responsible for many wells in an oil field, the accuracy and speed of visual troubleshooting of the sucker rod pump will be significantly affected. Therefore, the operational efficiency of the sucker rod pumping system can be greatly enhanced using machine learning techniques for automatic diagnosis. These techniques allow faster repairs and even preventive interventions, automatically identifying the sucker rod pump failures allows for anticipating the problems and taking early corrective and prevention measures for it. (Nazi et al. 1994)

4.2 Objective

The main objective of this work is to build two different neural network algorithms which are able to analyze the performance of the sucker rod pump via classifying a representative pump card into five different conditions. And by evaluating and testing the two networks, the objective is to assess their performance and to emphasize their effectiveness in automatically detecting and identifying whether a sucker rod pump is working properly or suffers from a specific problem.

5 Procedure

This study is divided into six modules. Each module has a big impact on the overall performance of any problem. These six modules are represented by Figure 18.

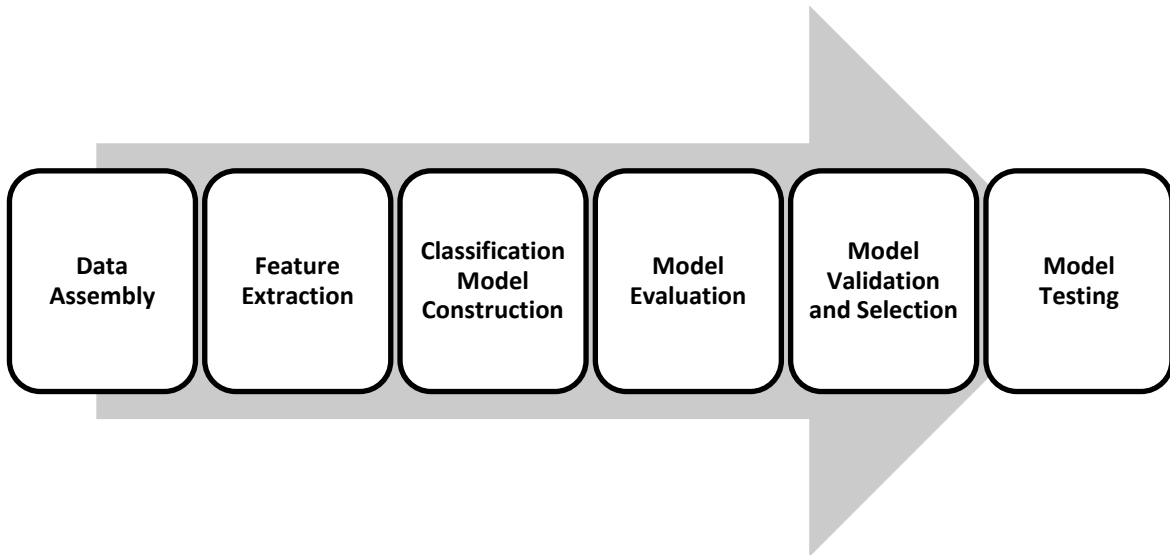


Figure 18: Machine learning procedure

Each module contains some steps. The work is found to be as follows:

- ✓ Collection of real field dynamometer cards which are pre-classified by experts.
- ✓ Selection of a feature extraction method and construction of its corresponding algorithm.
- ✓ Application of the feature algorithm to the gathered dynamometer cards.
- ✓ Splitting of the dataset into train and test data.
- ✓ Building of two types of neural networks.
- ✓ Evaluation of the two model's performance using specific metrics.
- ✓ Validation of the two models using a validation technique.
- ✓ Selection of the best model configuration for both networks.
- ✓ Testing of the two models against different pumping conditions.

Programming Software

This research requires programming processes. Thus, it needs certain software for that purpose. The deployed programming language is Python3, which is a well-known and powerful programming language in data analysis and in machine learning in general. Besides the programming language software, a programming library is required. A programming library which is called Keras was selected for this research since it contains all the required packages for constructing the BPNN and the CNN models.






6 Implementation of the procedure

As mentioned previously the procedure for analyzing sucker rod pump dynamometer cards consists of image data assembly, feature extraction, classification model construction, model evaluation, model validation, model selection and model testing.

6.1 Data Assembly

Data was collected from different fields in Brazil and it was provided by Prof. Dr. Leizer Schnitman from Electronic Engineering and Computing Department at the Federal University of Bahia in Brazil. The dataset consists of pre-classified 6132 dynamometer cards which represent five different pump conditions as shown in Table 2. This dataset will be spitted such as 80 % will be used for model training purposes and 20% will be deployed for model testing purposes.

Table 2: Dataset

Pump condition	Number of cards	Pump card example
Normal condition	1863	
Fluid pound	4120	
Plunger hitting up	48	
Leaking travelling valve	84	
Gas interference	17	

It is essential to point out that the gas interference pump cards are not reliable because they do not represent a gas interference condition besides the fact that its number is very low for model training purposes. It will be proved later that this category of pump cards will not be correctly classified by the networks, especially by the back propagation neural network.

6.2 Feature extraction

“In machine learning, pattern recognition and in image processing, feature extraction starts from an initial set of measured data and builds derived values intended to be informative and non-redundant, facilitating the subsequent learning and generalization steps, and in some cases leading to better human interpretations. Feature extraction is a dimensionality reduction process, where an initial set of raw variables is reduced to more manageable groups (features) for processing, while still accurately and completely describing the original data set.” (Wikipedia 2016)

There are important criteria for a feature extraction technique to be used (Rushin Shah 2014). In fact, a feature extraction technique must:

1. Reflect the nature of the data in a way that two images with the same shape must have the same descriptors.
2. Be stable in terms of invariance to rotation, scaling and translation.
3. Be robust against noise and distortion.
4. Capture critical relevancy, which means that the feature extraction technique should only contain information about what makes the analyzed object unique.

Elliptical fourier descriptors (EFDs) extraction, which is a technique that represents a closed contour by an n-dimensional feature vector which fully describe the whole card, was found to be the best feature extraction technique as it satisfies the above listed criteria.

Elliptical Fourier analysis (EFA) is a technique which extracts the EFDs coefficients of a chain-encoded contour. For this reason, the first step before the implementation of the EFA is to extract the dynamometer cards contour coordinates.

6.2.1 Dynamometer cards contour coordinates extraction

As mentioned previously, the pump card contour coordinates extraction is a necessary step before creating the elliptical Fourier descriptors. The contour of an image, based on the boundary pixels, can be represented by points which are characterized by (x,y) coordinates. Each column of the card image matrix is walked through until a first boundary pixel which is characterized by a non-zero value is found. From this pixel, the whole card contour is tracked by following the neighboring boundary pixels until all the boundary pixels are visited. At this point, a list of (x,y) positions of all the boundary pixels will be recorded. The resulting amount of points generated for each pump card is 101 points. Figure 19 represents an original pump card and its corresponding representation of its contour by boundary points.



Figure 19: Original pump card and pump contour with boundary points

6.2.2 Elliptical Fourier Descriptors implementation

The implementation of the EFD analysis requires several steps. (Frank P.Kuhl 1981)

1. Extracting the Boundary Chain representation

The previously determined (x,y) coordinates which represents a pump card contour is changed into their corresponding (x_p,y_p) which are defined as the links between every successive points. The sum of the links between the points can be computed from **eq.3** [10] and **eq.4** [10].

$$x_p = \sum_{i=1}^p \Delta x_i \quad (3)$$

$$y_p = \sum_{i=1}^p \Delta y_i \quad (4)$$

Where:

p: The index of the chain link.

x_p : Links summation on x-axis.

y_p : Links summation on y-axis.

2. Defining the Third Parameter

Afterwards, by assuming that the contour points are followed at a constant speed, a third parameter t_p , is defined, which is the required time to traverse the p links in the chain. It is represented by **eq.5** [10]

$$t_p = \sum_{i=1}^p \Delta t_i \quad (5)$$

Where:

P: The index of the chain link.

t_i : The time required to traverse a single link.

3. Elliptic Fourier coefficients extraction

Starting from a random point on the contour, the Fourier series representation is appropriate because the contour can be traveled through several times. The Fourier series expansion for the x projection of the chain code of the complete contour is defined as the sum of apparent displacements in x direction and it is represented by **eq.6** [10]:

$$x(t) = \sum_{n=1}^N \left[a_n \cos\left(\frac{2\pi n t}{T}\right) + b_n \sin\left(\frac{2\pi n t}{T}\right) \right] \quad (6)$$

Where:

T: The period (Summation of all T increments).

n: The number of the harmonic that we're looking at.

N: The total number of harmonics.

a_n, b_n : The Elliptic Fourier coefficients of the n^{th} harmonic.

The time derivative is periodic with period and can be represented by the Fourier series as in **eq.7** [10]

$$\dot{x}(t) = \sum_{n=1}^N \left[\alpha_n \cos\left(\frac{2n\pi t}{T}\right) + \beta_n \sin\left(\frac{2n\pi t}{T}\right) \right] \quad (7)$$

Where:

$$\alpha_n = \frac{2}{T} \int_0^T \dot{x}(t) \cos\left(\frac{2n\pi t}{T}\right) dt \quad (8)$$

$$\beta_n = \frac{2}{T} \int_0^T \dot{x}(t) \sin\left(\frac{2n\pi t}{T}\right) dt \quad (9)$$

$\dot{x}(t)$ is also obtained directly from its definition as:

$$\dot{x}(t) = \sum_{n=1}^N -\frac{2n\pi}{T} a_n \sin\left(\frac{2n\pi t}{T}\right) + \frac{2n\pi}{T} b_n \cos\left(\frac{2n\pi t}{T}\right) \quad (10)$$

The Elliptic Fourier coefficients are obtained by solving the two equations of $\dot{x}(t)$, **eq.11** [10] and **eq.12** [10].

$$a_n = \frac{T}{2n^2\pi^2} \sum_{p=1}^K \frac{\Delta x_p}{\Delta t_p} \left[\cos\left(\frac{2n\pi t_p}{T}\right) - \cos\left(\frac{2n\pi t_{p-1}}{T}\right) \right] \quad (11)$$

$$b_n = \frac{T}{2n^2\pi^2} \sum_{p=1}^K \frac{\Delta x_p}{\Delta t_p} \left[\sin\left(\frac{2n\pi t_p}{T}\right) - \sin\left(\frac{2n\pi t_{p-1}}{T}\right) \right]. \quad (12)$$

Where:

a_n, b_n : The Fourier coefficients of the n^{th} harmonic.

T: The period (Summation of all T increments).

n: The number of the harmonic that we're looking at.

K: The total number of links.

x_p : The sum of links on x-axis.

p: The index of the chain link.

t_p : The lengths of the chain at the path link.

The same procedures are applied for y direction. Accordingly, c_n and d_n are determined as shown in Equations **eq.13** [10] and **eq.14** [10].

$$c_n = \frac{T}{2n^2\pi^2} \sum_{p=1}^K \frac{\Delta y_p}{\Delta t_p} \left[\cos\left(\frac{2n\pi t_p}{T}\right) - \cos\left(\frac{2n\pi t_{p-1}}{T}\right) \right] \quad (13)$$

$$d_n = \frac{T}{2n^2\pi^2} \sum_{p=1}^K \frac{\Delta y_p}{\Delta t_p} \left[\cos\left(\frac{2n\pi t_p}{T}\right) - \cos\left(\frac{2n\pi t_{p-1}}{T}\right) \right] \quad (14)$$

Where:

c_n, d_n : The Fourier coefficients of the n^{th} harmonic.

T: The period (Summation of all T increments).

n: The number of the harmonic that we're looking at.

K: The total number of links.

y_p : The sum of links on y-axis.

p: The index of the chain link.

t_p : The lengths of the chain at the path links.

4. Machine Learning Input Vector construction

The number of selected elliptical Fourier descriptors is 15 and each descriptor provides 4 coefficients, a_n , b_n , c_n and d_n . Therefore, a matrix of $[15 \times 4]$ values is produced representing 60 EFDs coefficients. These 60 descriptors form a feature vector $X = (a_1, b_1, c_1, d_1, \dots, a_{15}, b_{15}, c_{15}, d_{15})$ which fully describes a selected pump card. As mentioned previously, this vector is used as an input to the back propagation neural network.

6.2.3 Fourier Descriptors Application

The generated elliptic Fourier descriptors showed good results in the pump card shape approximation. Figure 20 illustrates the results of the EFDs in approximating a fluid pound pump card with 15 harmonics. The approximated card is the last one in the right down corner of figure 20.

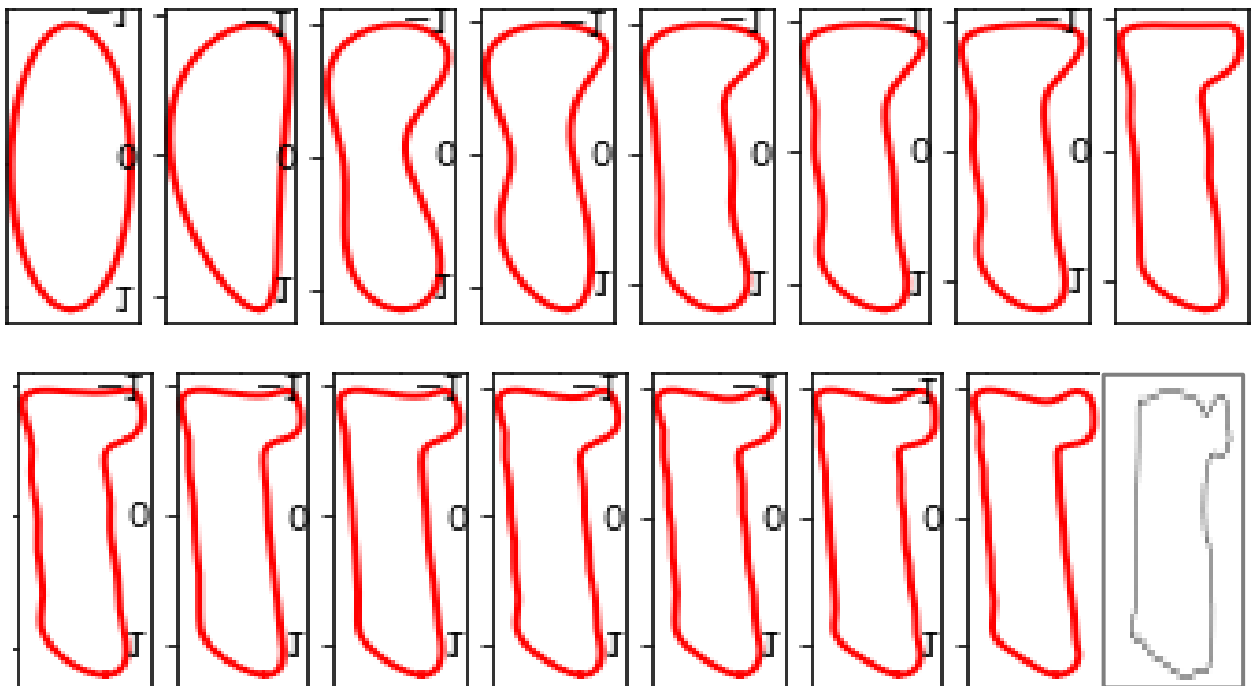


Figure 20: Constructed Elliptical Fourier descriptors

As it can be seen from Figure 20, the four terms of the elliptical Fourier spectrum, calculated over 15 harmonics, are sufficient to represent the dynamometer card shape with high accuracy. The number of harmonics should be properly selected to represent the most complex shape in the sample. (Frank P.Kuhl 1981)

6.3 Model Construction

Two types of artificial neural network are deployed to classify a sucker rod pump condition based on the shape of its dynamometer card. As mentioned previously, the aim of this work is to classify the dynamometer cards into five different classes. Different types of ANNs are applied in the field of images classification. In 2009, Alsmadi et al. concluded that the back propagation neural network is the best one among the multi-layer perceptron algorithms. (Suliman and Zhang 2015) However, convolutional neural network is the one known for its application in computer vision as it allows for direct image deployment without transforming it to a different descriptive form that has lower dimensionality. For this reason, these two networks were selected for building a pump cards classifier. The main difference between both networks lays in the network architecture and the ability of scaling to full images. In fact, in the case of BPNN, the input is a single vector which is transformed through a series of hidden layers. Each hidden layer has a set of independent neurons and each neuron is fully connected to all neurons in the previous layer, the output layer is a fully-connected layers and it represents the classification results. (Daphne Cornelisse 2018) Scaling to full images with significant dimensions is beyond the capability of a BPNN. In contrast to the CNN, this is possible because the network deploys 3D volumes of neurons. Meaning that, unlike the BPNN, the layers of a CNN have neurons arranged in 3 dimensions: width, height, depth. Moreover, For CNN, the neurons in a single layer is only connected to a small region of the layer before it, instead of all the neurons in a fully-connected way. At the end, the full image will be reduced into a single vector of class scores. Both networks will be later further described. Figure 21 illustrates the difference between a BPNN and a CNN in terms of network architecture. (Daphne Cornelisse 2018)

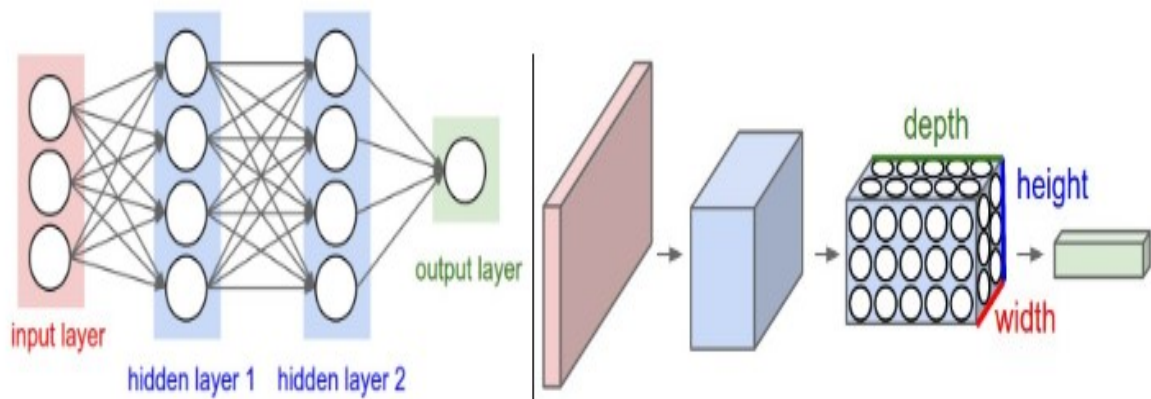


Figure 21 BPNN and CNN architecture [3]

6.3.1 Back propagation neural network

The back propagation neural network was first proposed by Paul Werbos in the 1970s and it was reviewed in 1986 by Rumelhart and McClelland, and after that back propagation became widely known and used. BPNN principle as well as its implementation procedure to construct a model for the dynamometer card five classes classification is presented. (Suliman and Zhang 2015)

6.3.1.1 Back propagation neural network Principle

Back propagation neural network is a bidirectional multi-layer neural network. As its name states, after generating an output value, the BPNN compares the actual input to the desired output. Then, it propagates the connection weights back to the input layer for adjustment in order to gradually correct the error. The connection weights adjustment stage is known as the network training process, which by the end of the execution stage, will be fixed and the network will be ready to directly calculate the outputs that correspond to a new input data. (Sidat Asiri) Figure 22 represents BPNN architecture.

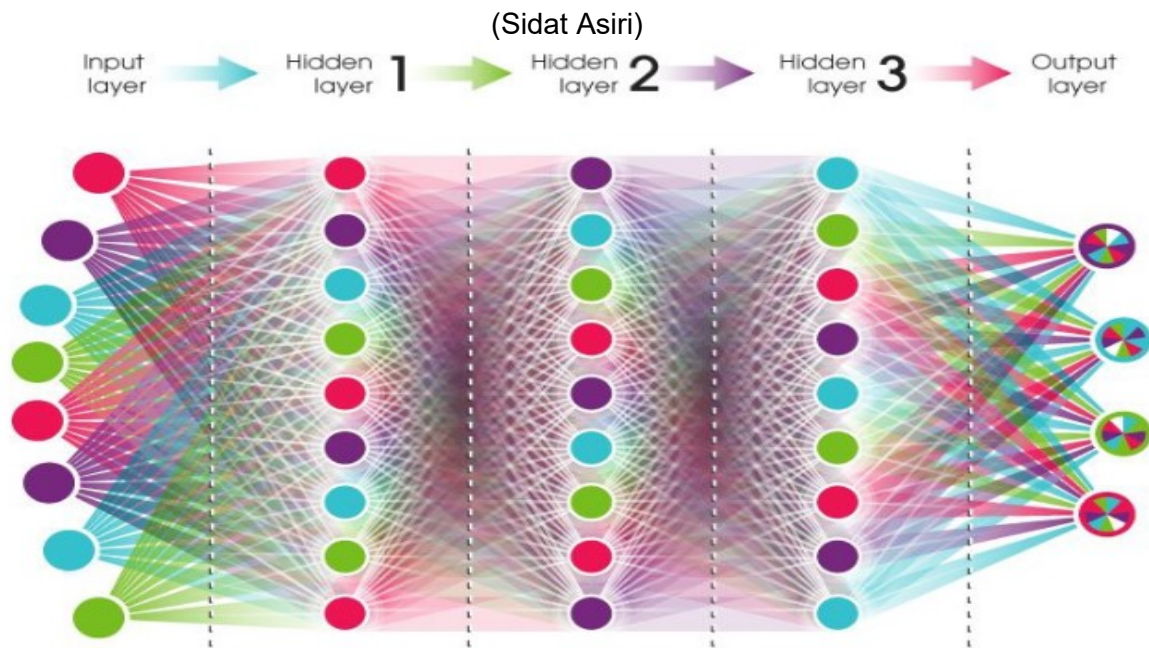


Figure 22: BPNN architecture [24]

The network consists of three types of layers:

1. The input layer which receives, scale and distribute the analyzed signal to the processing elements of the next layer.
2. The hidden layers which processes the inputs and sends the results to the output layer.
3. The output layer tells about the input image corresponding class.

For classification problems, usually, the number of input layer neurons corresponds to the number of the input images number bands and the number of the output neurons corresponds to the number of the predicted classes; however, the number of the hidden layer neurons and also the number of the hidden layers itself cannot be precisely determined because there is no rule or guideline to determine this number. (Suliman and Zhang 2015)

As mentioned before, the BPNN is a bidirectional network because it should be trained by examples before it can be used. The training process aims to adjust the connection weights and neurons thresholds by using training data sets. Figure 23 describe in detail a BPNN workflow.

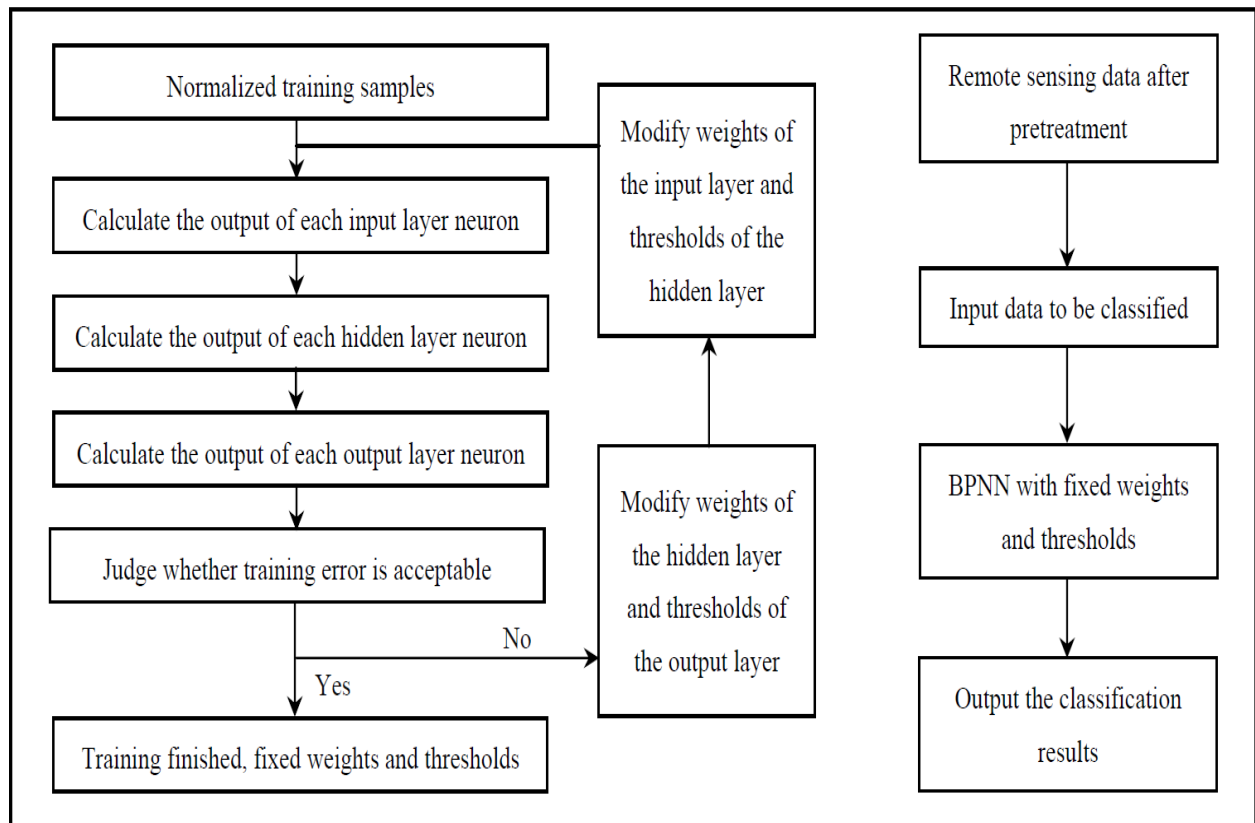


Figure 23: BPNN workflow [25]

The execution stage of the trained networks will be implemented by fixing the initial connection weights and thresholds. The normalized training samples are introduced into the input neurons where they are scaled and transferred to the hidden layer. The received input signals at the hidden layer neurons are processed to calculate an output which will be transferred to other neurons by an activation function. This process will continue from one layer to another until the actual output signals are produced at the last layer which contains the output neurons, where the training error is judged to be acceptable or not; if it is acceptable, the training is finished, and weights and thresholds are fixed. If not, the weights and thresholds are adjusted and fed to the network to start a new training cycle. (Suliman and Zhang 2015)

6.3.1.2 Back propagation neural network construction

In this work, the network input layer represents the input set which consists of the Elliptical Fourier descriptors, hence, the number of neurons in this layer is the same as the number of the (EFDs) and the output layer represents the five different classes to be predicted. And concerning the network hidden layer, both its number and its neurons number are chosen by trying different configurations and selecting the best one. Table 3 displays the number of neurons for each layer of the constructed ANN model.

Table 3: Constructed BPNN model configuration

Layer type	Number of neurons
Input layer	60
Hidden layer	100
Hidden layer	100
Hidden layer	100
Output layer	5

6.3.2 Convolutional neural network

Convolutional neural networks are a powerful type of neural network that is used primarily for image classification. (Nameer Hirschkind, Jyo Pari, Jimin Khim) The design of convolutional neural networks takes inspiration from the human visual cortex where visual information is processed. The visual cortex contains many receptors which detect light in overlapping regions of the visual field. Each receptor processes its input in the same way by the same convolution operation. CNN design is based on the same specifications. Similar to the back propagation neural network, Convolutional Neural Network is constituted of neurons that have learnable weights, but has a different architecture. (Joshi 2016)

6.3.2.1 Convolutional Neural Network Principle

The best way to understand CNN working principle is to explore its architecture which is represented by Figure 24:

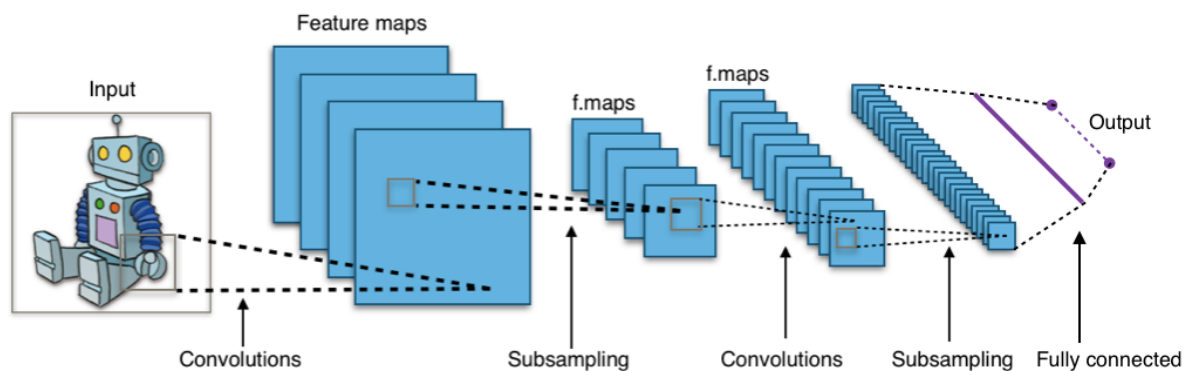


Figure 24: CNN architecture [29]

From Figure 24, it is clear that the network is constituted of 3 layers:

1. Convolution layer

The main function of the convolution layer is to collect the representative features of an image which is represented by a 2D-matrix characterized by a set of pixels which are contained into grids. Convolution multiplies this matrix by a filter or kernel which is represented by a 2D matrix with a selected dimension. The output representation is a feature map and the number of applied filters dictates the number of obtained feature maps. It is easier to visualize a filter as a window of a certain size sliding over the dimensions of an image and change each image pixel value as it goes. Figure 25 shows the convolution layer function. (Daphne Cornelisse 2018; Wikipedia 2019a)

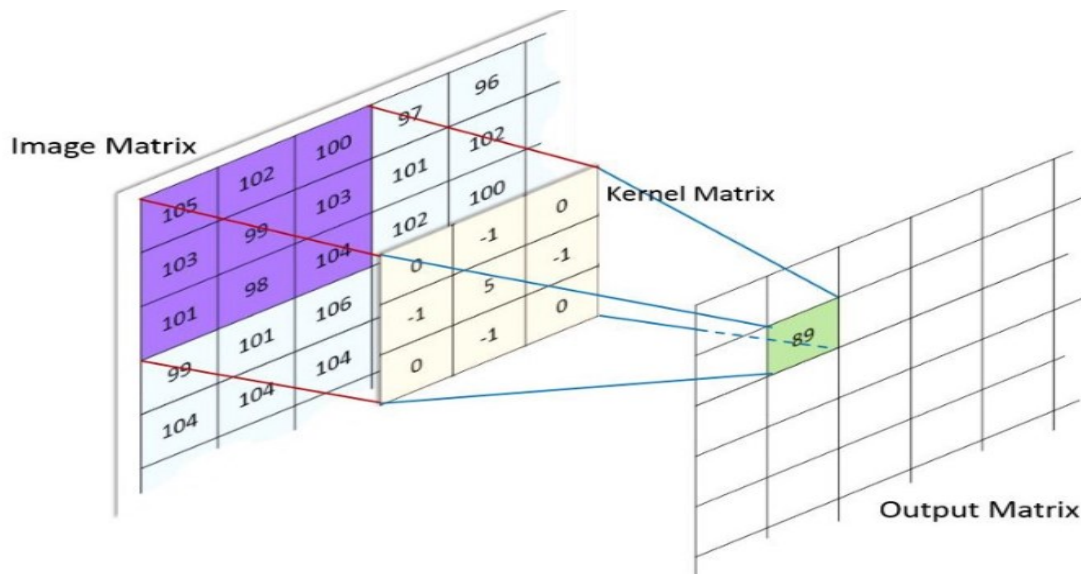


Figure 25: Convolution layer [16]

2. Pooling layer

Pooling layer performs a down-sampling operation on an input representation. The main common pooling is called max pooling, after dividing the operated input by splitting it into equal parts. It takes the maximum value from a selected region. (Wikipedia 2019d) The purpose of pooling is dimensionality reduction, which in turn helps in reducing computational load and prevent over-fitting which happen when the network memorizes the data instead of learning patterns in it. It shows perfect training results but fails when it is tested on a new data. Figure 26 will clarify this idea; each color box within the matrix represents a subsample. (Daphne Cornelisse 2018)

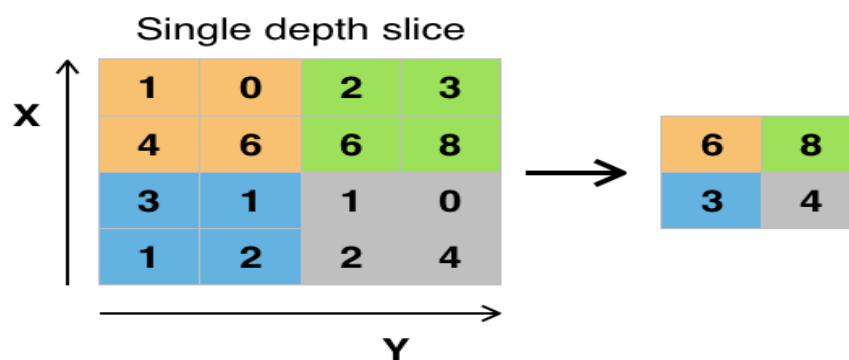


Figure 26: Pooling layer [29]

3. Fully Connected layer

The fully connected layer is a regular feed-forward network which produces the output containing the classification result.

❖ Additional layer which is the flatten layer, is required between the last pooling or convolution layer and the fully connected layer. It flattens the output from the previous layer by converting it from a matrix representation to a vector representation.

6.3.2.2 Convolutional Neural Network Construction

The Constructed CNN in this research is based on the previously described workflow. Table 4 and 5 Table represent the network set parameters and the network architecture respectively.

Table 4: CNN setting parameters

Parameter	Size
Input image dimensions	(96,112)
Number of filters	32
Filter size	(3,3)
Pooling area for max pooling size	(2,2)

Table 5: Constructed CNN model architecture

Type of layer	Activation function
Convolution	Relu
Pooling layer	-
Convolution layer	Relu
Pooling layer	-
Flattening layer	-
Fully connected layer	Softmax

The input dynamometer cards to the network are characterized by a matrix composed of 96 rows and 112 columns, which will be convolved with 32 filters having a size of (3,3). Afterwards, the output image matrix will be pooled with a pooling area size of (2,2). The network is composed of 6 layers: 2 convolution layers, 2 pooling layers, a flattening layer and a fully connected layer. Concerning the activation function, Relu function is used for the convolution layer because, logically if the convolution layer collects features inside the image by looking if the pixel is present or not within the visited grid, it is convenient to use a function that returns 0 if it receives any negative input and it returns the value back if it encounters any positive value x . However, Softmax function is used for the fully connected output layer since it is a function that takes as input a vector of K real numbers, and normalizes it into a probability distribution consisting of k probabilities. (Wikipedia 2019c)

6.4 Model Evaluation

After creating the two models, it is convenient to evaluate them. The addressed property which is evaluated is the accuracy which is simply the proportion of correctly classified dynamometer cards. For this purpose, confusion matrix and precision, recall and F1 score are deployed.

6.4.1 Confusion matrix

Confusion matrix is a specific table that allows for the evaluation of artificial neural network models accuracy by visualizing the proportion of correct classifications. The matrix has two-dimensions; one dimension is indexed by the target class while the other is indexed by the predicted class (or vice versa). Figure 27 represents presents a typical confusion matrix layout for a multi-class classification task, with the classes A_i and $i=1\dots n$. In the confusion matrix, N_{ij} represents the number of samples belonging to class A_i but classified as class A_j . Confusion matrices of this research relative to the two constructed networks are illustrated in the section of model validation and selection. (Deng et al. 2016)

		Predicted			
		A_1	... A_j ...	A_n	
Actual	A_1	N_{11}	N_{1j}	N_{1n}	
	\vdots		\vdots		
	A_i	N_{i1}	... N_{ij} ...	N_{in}	
	\vdots		\vdots		
	A_n	N_{n1}	N_{nj}	N_{nn}	

Figure 27: Confusion matrix [5]

In this work, there are five pump cards classes:

1. Normal condition (N)
2. Leaking travelling valve (TV)
3. Hitting up plunger (HP)
4. Gas interference (GI)
5. Fluid pound (FP)

Figure 28 shows an example of a constructed confusion matrix resulted by the BPNN on the test set. When we focus on the matrix rows; in the first row, the network has classified one card as a fluid pound which is a normal condition. In the third row, the network classified the entire 12 hitting up condition cards correctly. In contrast to the forth row, where the network failed to classify all the gas interference condition cards. This, as mentioned from the beginning, is due to the low quality of the cards representing the gas interference since they represent normal condition instead of gas interference condition. In addition, the small number of cards belonging to that category prevents the network from being well trained to recognize this class. Figure 29 represents an example of a constructed confusion matrix resulted by the CNN on the test set also. It shows that the CNN in this example succeeded in predicting correctly almost all the cards.

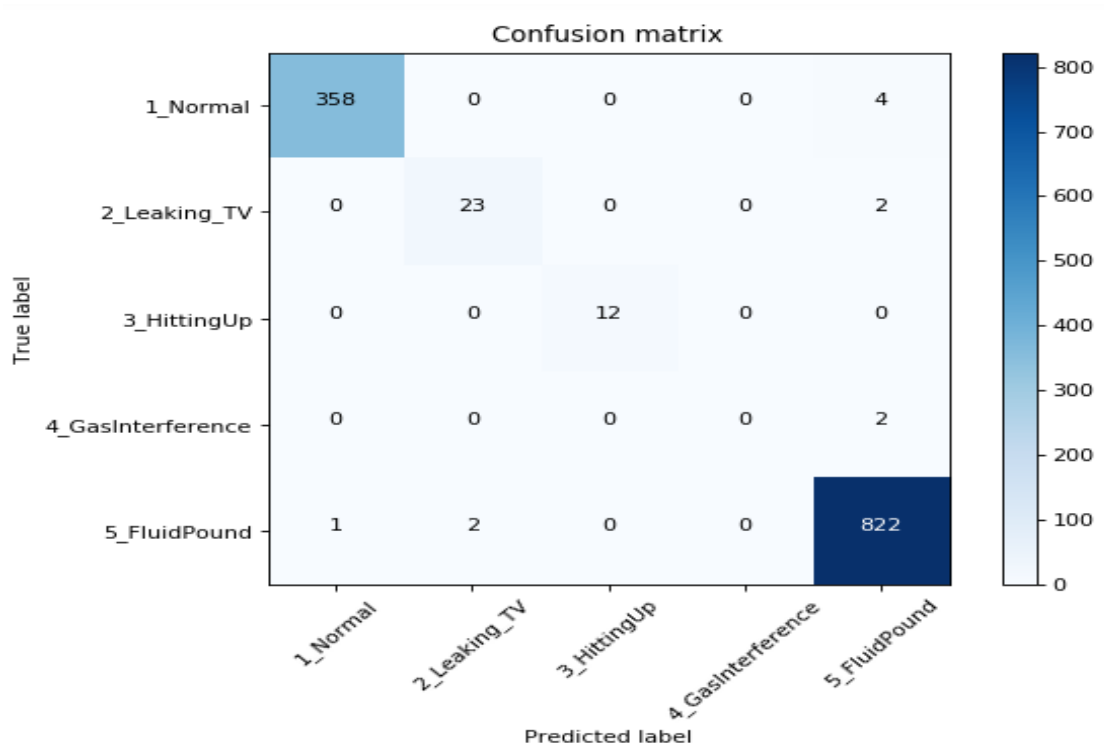


Figure 28: BPNN confusion matrix

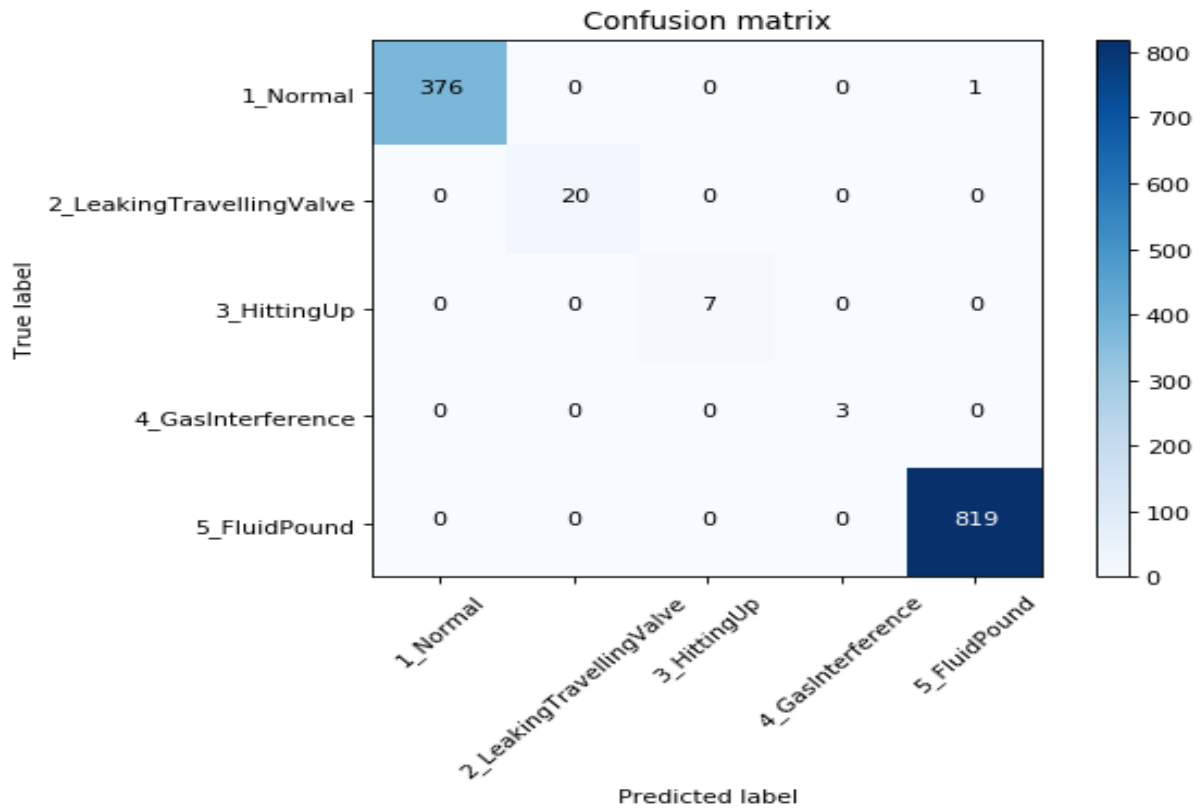


Figure 29: CNN confusion matrix

6.4.2 Precision, recall and F1 score

In order to describe precision recall and F1 score, it is convenient to define the generalized version of the confusion matrix which is a binary confusion matrix. It is for instance a two by two table which includes four outputs produced by a binary classifier which means that class labels can take only two possible values: positive or negative. The correctly and incorrectly positive predicted classes are called true positives and false positives, respectively. Similarly, the correctly and incorrectly negative predicted classes are called true negatives and false negatives. Table 6 shows a binary confusion matrix layout which simply contains the number of instances that belongs to one of these four categories. (Wikipedia 2019d)

Table 6: Binary Confusion Matrix [23]

Results	Actual class 1	Actual class 0
Predicted class 1	True Positive	False Positive
Predicted class 0	False Negative	True Negative

The precision is the ratio of the number of relevant extracted records to the total number of irrelevant and relevant extracted records, and in our case, it represents the percentage of the number of cards with a certain condition which are correctly classified out of the correctly and incorrectly predicted cards. **Eq.15** [22] represents the mathematical form of the Precision. (Shruti saxena 2018)

$$\text{precision} = \frac{\text{True positive}}{\text{True positive} + \text{false positive}} \quad (15)$$

The recall is the ratio of the number of relevant extracted records to the total number of the relevant extracted records in the database and it represents in our case the percentage of the number of cards which are correctly classified out of all the cards specific to the predicted condition. **Eq.16** [22] represents the mathematical form of the Recall.

$$\text{Recall} = \frac{\text{True positive}}{\text{True positive} + \text{false negative}} \quad (16)$$

Precision is a measure of how good predictions are with regard to false positives whereas the recall is a measure of how good the predictions are with regard to false negatives. F1- score is a third parameter which can be derived from the precision and recall and the higher the F1-score is, the higher the accuracy of the network is. (Sarang Narkhede 2018)

F1-score is computed based on **eq.17** [22]

$$F_1 = 2 * \frac{\text{Precision} * \text{Recall}}{\text{Precision} + \text{Recall}} \quad (17)$$

Figure 30 and Figure 31 represents a plot which displays the precision, recall and F1 score relative to the illustrated confusion matrices in the previous section for the BPNN and for the CNN respectively.

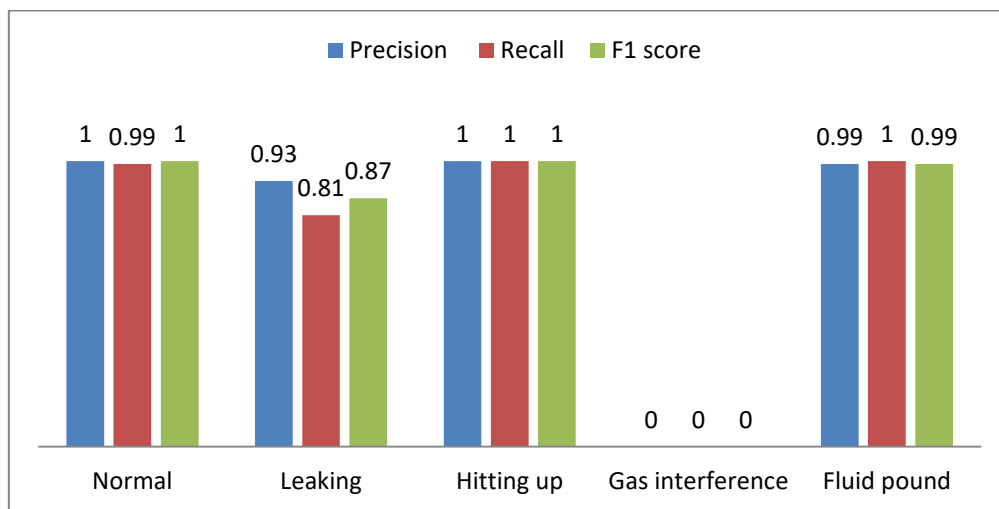


Figure 30: Precision, recall and F1- Score for BPNN

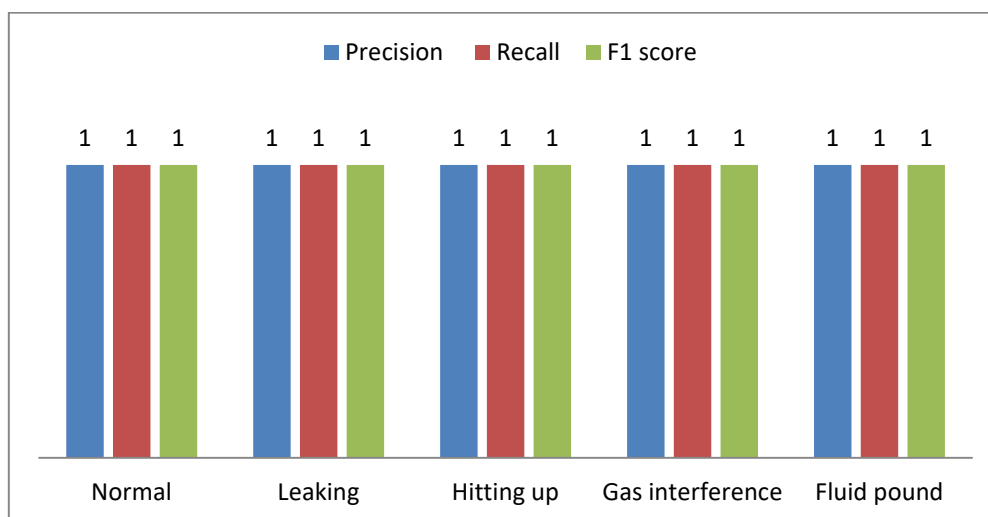


Figure 31: Precision, recall and F1-score for CNN

When comparing the two graphs of precision, recall and F1-score to their corresponding confusion matrices, it is easy to notice that the two results match each other. In fact, the perfect prediction results of the CNN are reflected by Figure 31, where the precision, recall and F1-score are perfect too (equal to one). For the case of the BPNN, as mentioned previously, the gas interference condition is not predicted at all which is proved by the zero value of the precision, recall and F1-Score. Regarding the hitting up plunger condition, which was perfectly predicted based on the confusion matrix, the precision, recall and F1-score value which is 1 confirmed this perfect prediction. Concerning the other three conditions, they showed good results in the confusion matrix and with the precision, recall and F1-score as well.

6.5 Model Validation and Selection

Model validation is a method for checking the stability of our constructed neural network models. Both the BPNN and the CNN are validated by k-fold cross validation. The advantage of K-Fold cross validation method is that there is no necessity to remove a part of the data for validation which may cause the loss of important patterns from the dataset. Later, model selection is an automatic method to find a further optimized model.

6.5.1 K-Fold Cross-Validation

Cross-validation is a resampling procedure which is used to evaluate the skill of a machine learning algorithm on unseen data. Its governing parameter to be chosen is the denoted k which refers to the number of groups that a given data is to be divided into. This approach involves randomly dividing the set of observations into k groups, or folds, of equal size. The first fold is treated as a validation or testing set and the model is fit on the remaining $k - 1$ parts. Figure 32 illustrates the splitting of the data into k parts. (Matthew Terrible 2017)

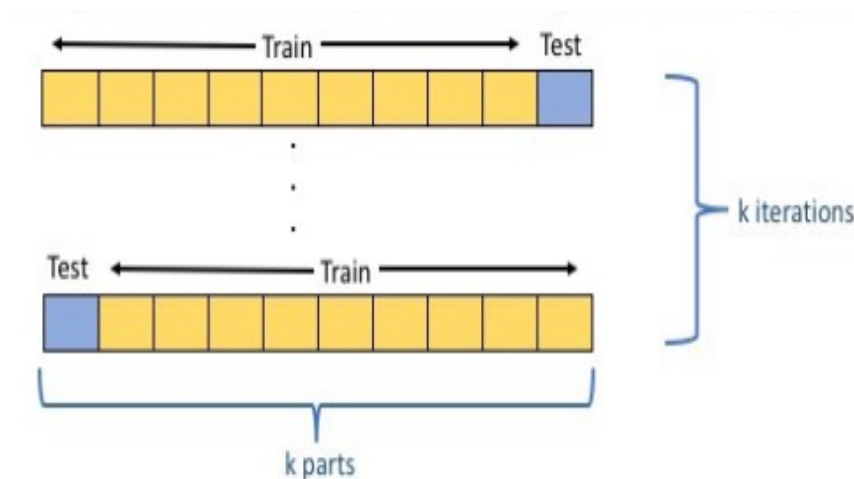


Figure 32: K-Fold cross validation [15]

“The choice of k is usually 5 or 10, but there is no formal rule. As k gets larger, the difference in size between the training set and the resampling subsets gets smaller. As this difference decreases, the bias of the technique becomes smaller.” (Jason Brownlee 2018)

For this reason, the K value in this work was selected as 5 because three out of the five analyzed conditions have a small dataset and it is convenient to deploy 5 k value instead of 10.

The k-fold cross validation procedure in this research is represented by Figure 33 and is as follows: (Jason Brownlee 2018)

1. The dataset is split into 5 parts.
2. 1 part out of 5 of the datasets, which is represented by blue color in Figure 33, was taken as a test dataset and the remaining 4 parts, which are represented by red color was attributed to the training data set.
3. The model is fitted on the training set and evaluated on the test set.
4. The test set is rotated 5 times and the previous steps are repeated.
5. For each iteration, evaluation metrics as the precision, recall and F1 score and the confusion matrix are retained. (Eijaz Allibhai 2018)



Figure 33: 5-Fold cross validation [8]

6.5.2 Model Selection

Model selection is done by creating a loop function which creates three different models for each cross-validation round, from which the best model is selected based on its corresponding F1-Score and then it is saved. The model which has the highest value of F1-score is the one to be selected. We have five cross validation rounds and two types of neural networks: the BPNN and the CNN. Three models are generated at each cross-validation step and one of the three models is selected. As a result, 30 models are generated, and 10 models are selected and saved. The loop function chooses the best model from a list of candidate models following the workflow which is described by Figure 34:

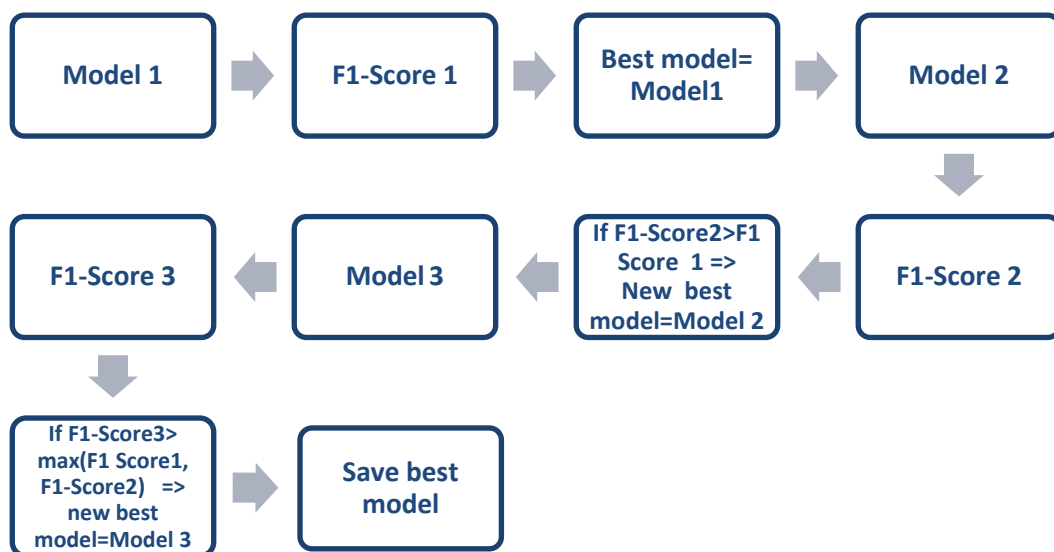


Figure 34: Model selection procedure

First model is created by setting the initial weights of the network. Then, the accuracy of the model is estimated by the F1-score. The computed F1-score of the first model is assumed to be the highest value which means that model 1 is set to be the best model at the beginning of the process. A second model is created by changing the initial network weights and its corresponding F1-score is calculated. At this stage, if the new F1-score value is higher than the previous one, the second model is assigned to be the new best model; otherwise, the best model will remain assigned to the first model. Similarly, a third model is created, and its F1-Score is computed. If the new F1-Score value is higher than the two previous F1-Score values, model 3 will be the new best model. Finally, the selected best model is saved in order to be loaded later for testing.

6.6 Model testing

After building the BPNN and the CNN, the two models are saved to be loaded later for testing over different five dynamometer cards in order to check their performance. The five following figures display one card for each pump condition with the corresponding true label, predicted label and the result of the prediction if it is correct or false.

6.6.1 Back Propagation neural network testing

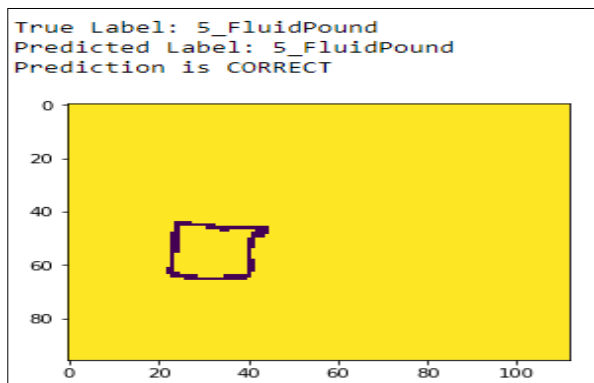


Figure 35: Fluid pound card testing

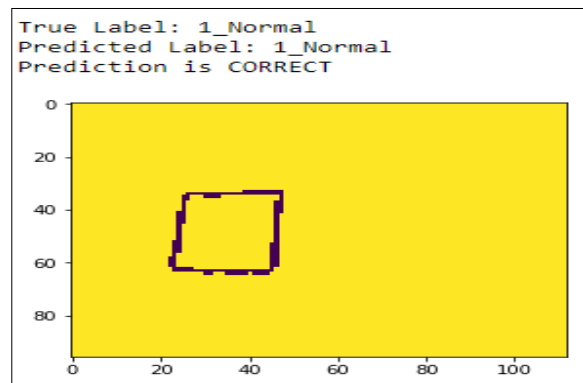


Figure 36: Normal card testing

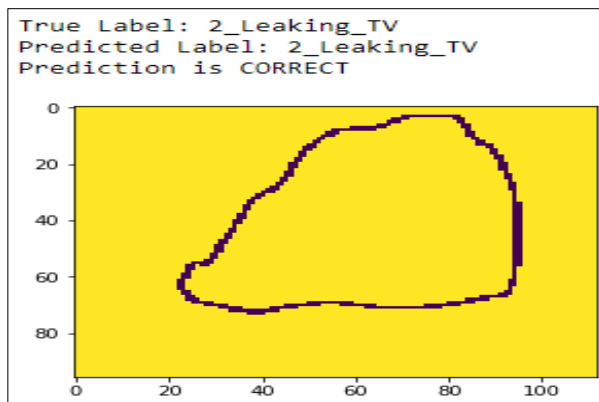


Figure 37: Hitting up card testing

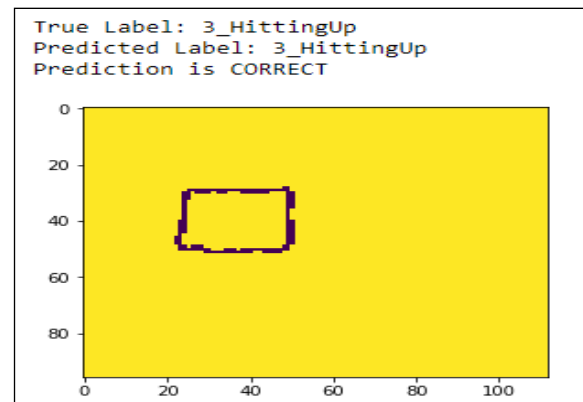


Figure 38: Leaking TV card testing

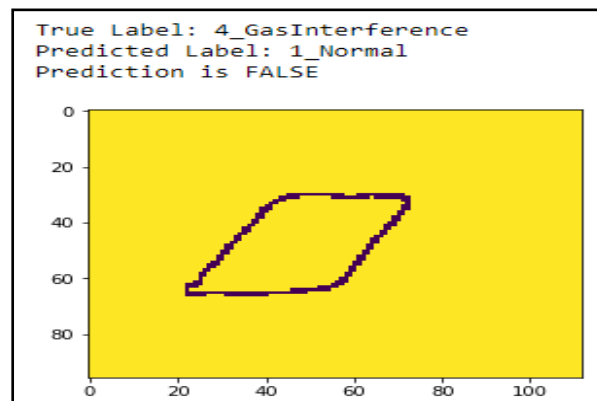


Figure 39: Gas interference card testing

6.6.2 Convolutional neural network testing

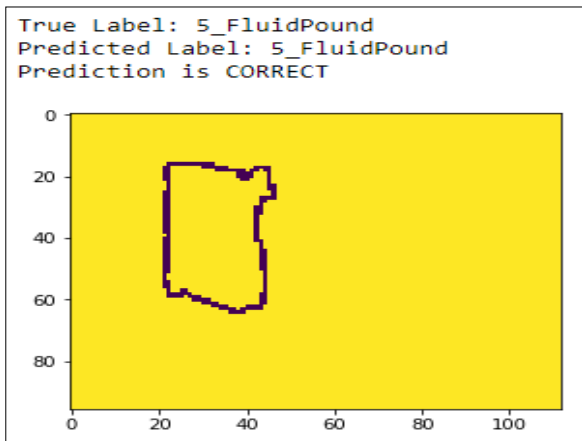


Figure 40: Fluid pound card testing

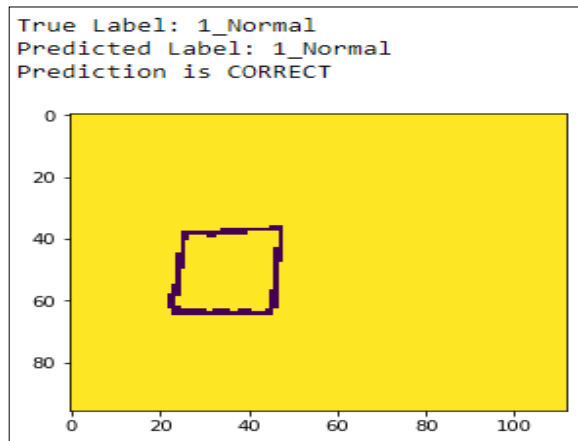


Figure 41: Normal card testing

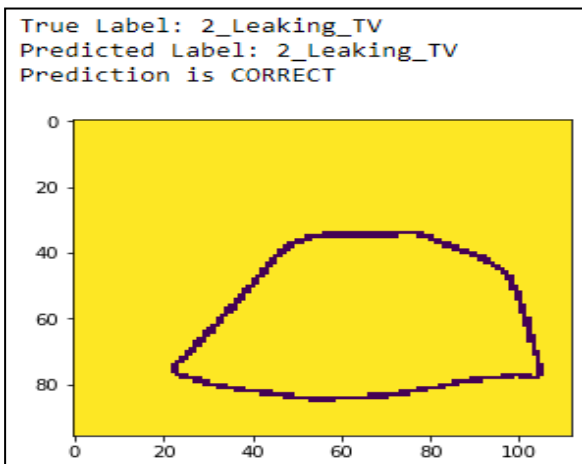


Figure 42: Leaking TV card testing

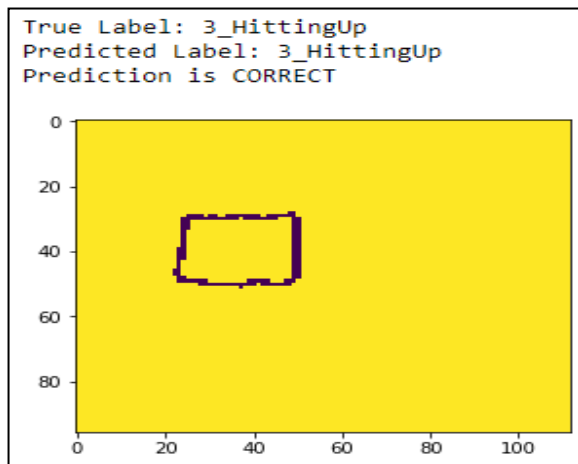


Figure 43: Hitting up card testing

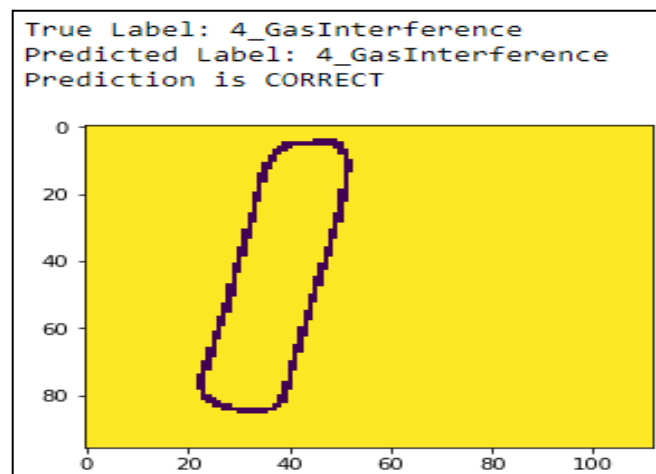


Figure 44: Gas interference card testing

7 Results and Discussion

7.1 Results

The results are displayed for the back propagation neural network and the convolutional neural network.

7.1.1 Back Propagation Neural Network results

Table 7: Back propagation neural network results

X-Val		N	LTV	HU	GI	FP	N	LTV	HU	GI	FP	N	LTV	HU	GI	FP
1	N	376	0	0	0	4	374	2	0	0	3	373	0	0	0	4
	LTV	0	20	0	0	0	0	20	0	0	0	0	20	0	0	0
	HU	0	0	7	0	0	0	0	7	0	0	0	0	7	0	0
	GI	0	0	0	0	3	0	1	0	0	2	0	0	0	0	3
	FP	1	0	0	0	818	2	0	0	0	817	2	0	0	0	817
			F1-Score = 0.8					F1-Score = 0.79					F1-Score = 0.8			
2	N	359	2	0	0	3	357	2	0	0	5	356	1	0	0	5
	LTV	0	25	0	0	0	0	25	0	0	0	0	25	0	0	0
	HU	0	0	12	0	0	0	0	12	0	0	0	0	12	0	0
	GI	0	1	0	1	0	0	0	0	1	1	0	2	0	0	3
	FP	2	3	0	1	819	2	0	0	0	823	3	5	0	0	817
			F1-Score = 0.88					F1-Score = 0.93					F1-Score = 0.77			
3	N	360	0	0	0	2	361	2	0	0	1	393	0	0	0	2
	LTV	1	10	0	0	5	0	16	0	0	3	0	10	0	0	5
	HU	0	0	10	0	0	0	0	10	0	0	0	0	10	0	0
	GI	1	0	0	0	1	1	0	0	0	1	1	0	0	0	1
	FP	4	0	0	0	832	6	3	0	0	827	4	0	0	0	832
			F1-Score = 0.75					F1-Score = 0.78					F1-Score = 0.77			
4	N	393	2	0	0	7	395	2	0	0	5	399	2	0	0	1
	LTV	0	8	0	0	0	0	8	0	0	0	0	8	0	0	0
	HU	0	0	6	0	0	0	0	6	0	0	0	0	6	0	0
	GI	2	0	0	0	7	3	0	0	0	6	3	3	0	0	3
	FP	2	0	0	0	799	3	0	0	0	798	3	1	0	0	797
			F1-Score = 0.77					F1-Score = 0.77					F1-Score = 0.74			
5	N	350	0	0	0	9	350	0	0	0	9	353	2	0	0	6
	LTV	0	12	0	0	3	0	12	0	0	3	0	15	0	0	0
	HU	0	0	13	0	0	0	0	13	0	0	0	0	13	0	0
	GI	0	0	0	0	1	0	0	0	0	1	0	1	0	0	0
	FP	0	3	0	0	835	0	3	0	0	835	0	2	0	0	836
			F1-Score = 0.76					F1-Score = 0.76					F1-Score = 0.78			

7.1.2 Convolutional Neural Network results

Table 8: Convolutional Neural Network results

X-Val																
		N	LTV	HU	GI	FP	N	LTV	HU	GI	FP	N	LTV	HU	GI	FP
1	N	362	0	0	0	1	376	0	0	0	1	396	0	0	0	1
	LTV	0	25	0	0	0	0	20	0	0	0	0	20	0	0	0
	HU	0	0	12	0	0	0	0	7	0	0	0	0	7	0	0
	GI	0	0	0	2	0	0	0	0	0	2	0	0	0	3	0
	FP	0	0	0	0	819	0	0	0	0	819	1	0	0	0	818
			F1-Score = 0.99					F1-Score = 0.99					F1-Score = 0.99			
2	N	362	0	0	0	0	362	2	0	0	0	362	1	0	0	0
	LTV	0	25	0	0	0	0	25	0	0	0	0	25	0	0	0
	HU	0	0	12	0	0	0	0	12	0	0	0	0	12	0	0
	GI	0	0	0	2	0	0	0	0	2	1	0	2	0	2	0
	FP	2	0	0	0	823	1	0	0	0	824	1	0	0	0	824
			F1-Score = 0.99					F1-Score = 0.99					F1-Score = 0.99			
3	N	362	0	0	0	0	362	2	0	0	0	362	2	0	0	0
	LTV	0	16	0	0	0	0	16	0	0	0	0	16	0	0	0
	HU	0	0	10	0	0	0	0	10	0	0	0	0	10	0	0
	GI	0	0	0	2	0	0	0	0	2	0	0	0	0	2	0
	FP	0	0	0	0	836	0	0	0	0	836	0	0	0	0	836
			F1-Score = 1					F1-Score = 1					F1-Score = 1			
4	N	402	0	0	0	0	402	0	0	0	0	402	0	0	0	0
	LTV	0	16	0	0	0	0	8	0	0	0	0	8	0	0	0
	HU	0	0	6	0	0	0	0	6	0	0	0	0	6	0	0
	GI	2	0	0	6	1	0	0	0	8	1	0	0	0	8	1
	FP	0	0	0	0	801	0	0	0	0	801	0	0	0	0	801
			F1-Score = 0.96					F1-Score = 0.99					F1-Score = 0.99			
5	N	358	0	0	0	1	358	0	0	0	1	358	0	0	0	0
	LTV	0	15	0	0	0	0	12	0	0	0	0	15	0	0	0
	HU	0	0	13	0	0	0	0	13	0	0	0	0	13	0	0
	GI	0	0	0	1	0	0	0	0	1	0	0	0	0	1	0
	FP	0	0	0	0	838	0	0	0	0	838	1	0	0	0	838
			F1-Score = 0.99					F1-Score = 0.99					F1-Score = 0.99			

7.2 Discussion

Results for both networks are displayed by table 7 and table 8. Both tables contain the confusion matrices of the three created models for each cross-validation round for the two networks (BPNN and CNN). The tables show also the F1-Score value related to each confusion matrix. The F1-Score, as described in the section of model selection, is the parameter on which the network is based on to decide which model out of the constructed three ones has performed better. When comparing the two tables. The F1-Score, which are highlighted in the tables, correspond to the best selected model based on the model selection workflow which was described previously.

7.2.1 BPNN and CNN comparison

The BPNN model has been developed and optimized with several scenarios of different number of layers, number of nodes (only in the hidden layer as the input and output layer nodes number is fixed as mentioned previously), activation functions and initial weights value. For the CNN case, the same thing has been done by trying different number of filters; filter dimensions, number of convolution and pooling layers, activation functions and different pooling area sizes. Each case during this study produced different results, which has achieved different prediction accuracies. Therefore, the program must be designed and optimized in such a way that it can produce the best prediction by combining the most optimum parameters. The network configuration of both CNN and BPNN, which results in the best performance in terms of accuracy, has been retained to be evaluated, validated and tested. The model evaluation was performed by generating the confusion matrices of the prediction results. Precision recall and F1-score was also analyzed for each pump card category. Concerning the validation, it was performed by the cross validation with five iterations to validate the model stability and reliability. The testing is just the application of the constructed model on different dynamometer cards with different classes and visualization of the model output, which will tell each time if the prediction is correct or not. Until now, it seems to be that the best model has been selected. However, an alternative work has been done to optimize the retained model. This work consists of generating three models which differ just in terms of the initial weights, at each cross-validation step. Then, prediction results of the three models were compared to retain the best model and discard the two others. Table 7 and Table 8 summarize these results. It is obvious that the convolutional neural network has a better performance than the back propagation neural network. The BPNN accuracy range is between 0.76 and 0.93 and the CNN accuracy varies from 0.96 and 1. The source of this important difference in terms of accuracy is the working principle of the two networks. Indeed, which makes the CNN way better is the fact that it analyzes the dynamometer cards as they are, and it does not demand an alternative representation of the cards to be used for learning and testing. However, the BPNN requires an additional representation with less dimensionality. In this work, this was given by the elliptical Fourier coefficients vector which represents the cards in a different form. It can be noticed from the confusion matrices, that the gas interference condition, especially with BPNN, is not predicted at all most of the times. This, as mentioned from the beginning, is because of the small size of data which represent this condition. Moreover, the gas interference cards are not reliable, not only because of the dataset small size, but also because they do not correspond to the label attributed to them. In contrast to the CNN, which in many instances, showed its ability to predict that condition class. This is due the CNN principle which works by analogy with the human visual cortex. In addition, it is obvious that the five cross

validation produced good outputs and there is no fluctuation in terms of the prediction results which may indicate that the two models are not stable and cannot be reliable. However, the CNN showed better stability, not only because the five cross validation results are convenient, but also because even among the three created models at the same cross validation round. Since the two models produced very good results for the BPNN and excellent results for the CNN, and this is due to the working principle of the two networks and not because of the model's configuration. It is convenient to make recommendations regarding the dataset.

7.2.2 Recommendations

Since the data quality directly affects the model classification prediction results, class labels for each card, size of the datasets as well as data distribution, should be attributed a primary concern. In fact, small dataset as well as a non-descriptive data and non-equally distributed data classes along the dataset will affect both the training of the network. And as the testing process is based on the training phase, the prediction efficiency may not be reasonable. Moreover, in this research, the dataset was divided only into a training and test set and there was not some data retained for testing the model on a new pump cards which are never encountered by the network. In this work, this is not done because the data classes are not equally classified among the dataset and there are classes, for example gas interference and hitting up plunger conditions, which have a small number of cards. However, generally it is recommended to keep a part of the dataset from the beginning to assess the model skill on a new data.

Conclusion

Although this study involves several findings, the followings are the most important points and conclusions of this research:

1. The traditional concept of manually visualizing the sucker rod pump card is time and effort consuming and it does not cope with the automatic data generation technology. Therefore, automated diagnosis of pumping systems is a must nowadays.
2. A descriptive representation for the dynamometer cards was constructed. In this research, it is the elliptical Fourier descriptors.
3. Two models have been developed to classify five downhole pumping conditions of the sucker rod pump using Artificial Neural Networks (ANN). These two models are the back propagation neural network and the convolutional neural network.
4. Different networks setups were evaluated until the best configuration was reached for both types of networks.
5. Models with best configurations were investigated in terms of stability and reliability by a model validation technique.
6. Optimization procedure has been implemented to construct the most powerful ANN models.
7. This research has proved that machine learning techniques are able to predict the sucker rod pump condition with high accuracy which was in this work, 96% for BPNN and 100% for the CNN.
8. The results have shown that the convolutional neural network (CNN) is more accurate than the Back propagation Neural Network (BPNN).

List of Tables

Table 1: Typical pump cards [27, p.489].....14

Table 2: Dataset.....31

Table 3: Constructed BPNN model configuration.....39

Table 4: CNN setting parameters42

Table 5: Constructed CNN model architecture42

Table 6: Binary Confusion Matrix [23].....45

Table 7: Back propagation neural network results52

Table 8: Convolutional Neural Network results53

List of Figures

Figure 1: Usage of Artificial Lift Systems Worldwide [18]	1
Figure 2: Sucker rod pump working principle [26, p. 62]	3
Figure 3: Sucker rod pump system structure [18]	3
Figure 4: An echo-meter fluid level trace [6]	7
Figure 5: Sucker rod pumping unit failure fault tree representation [34, p. 111]	11
Figure 6: Sucker rod pump tubing failures fault tree representation [34, p. 112]	11
Figure 7: Sucker rod pump rod string failures fault tree representation [34, p. 113]	12
Figure 8: Sucker rod subsurface pump failures fault tree representation [24, p. 114].....	12
Figure 9: Reference pump card [26, p. 333]	13
Figure 10: Instrumented sucker rod pumping system [1]	18
Figure 11: position switch rod load sensor [1].....	19
Figure 12: Sucker rod pump off control diagram [33, p. 7]	20
Figure 13: SCADA system architecture [33, p.4]	22
Figure 14: production system of a rod pumped well [27, p. 398]	24
Figure 15: System performance curve sheet for a pumping system with a C 228D-213-100 unit, a 1.25 in plunger, API 86 rod string and Grade D rods [27, p. 403].....	25
Figure 16: Arrangement of POC and VSD devices for pumping speed control [27, p. 416]...28	
Figure 17: Operational principle of a well manager unit [27, p. 417].....28	
Figure 18: Machine learning procedure	30
Figure 19: Original pump card and pump contour with boundary points	32
Figure 20: Constructed Elliptical Fourier descriptors.....	35
Figure 21 BPNN and CNN architecture [3]	36
Figure 22: BPNN architecture [24].....	37
Figure 23: BPNN workflow [25].....	38
Figure 24: CNN architecture [29]	40
Figure 25: Convolution layer [16].....	41
Figure 26: Pooling layer [29].....	41
Figure 27: Confusion matrix [5].....	43
Figure 28: BPNN confusion matrix	44
Figure 29: CNN confusion matrix.....	44

Figure 30: Precision, recall and F1- Score for BPNN	46
Figure 31: Precision, recall and F1-score for CNN.....	46
Figure 32: K-Fold cross validation [15]	47
Figure 33: 5-Fold cross validation [8].....	48
Figure 34: Model selection procedure.....	49
Figure 35: Fluid pound card testing	50
Figure 36: Normal card testing	50
Figure 37: Hitting up card testing.....	50
Figure 38: Leaking TV card testing.....	50
Figure 39: Gas interfetrence card testing.....	50
Figure 40: Fluid pound card testing	51
Figure 41: Normal card testing	51
Figure 42: Leaking TV card testing	51
Figure 43: Hitting up card testing.....	51
Figure 44: Gas interference card testing.....	51

Abbreviations

ANN	Artificial Neural Network
BPNN	Back Propagation Neural Network
CNN	Convolutional Neural Network
EFDs	Elliptical Fourier Descriptors
EFA	Elliptical Fourier Analysis
SCADA	Supervisory Control and data Acquisition
LACT	Lease Automatic Custody Transfer
POC	Pump-off Controller
MTU	Master Remote Unit
RTU	Remote Terminal Unit
DBMS	Database Management System
GUI	Graphical User Internet
WSN	Wireless Sensor Networks
DBR	Dynamic Braking Resistor
VSD	Variable Speed Drive
X-VAL	Cross Validation
N	Normal
LTV	Leaking Travelling Valve
HU	Hitting Up
GI	Gas Interference
FP	Fluid Pound
TV	Travelling Valve
SV	Standing Valve

References

- [1] Anthony Allison (2015): Accurate Load & Position Measurement Is Critical to Quality Dynamometer Analysis. Weatherford, updated on 9/18/2015, checked on 1/22/2019.
- [2] Corsano, Alfred (1994): Application of Artificial Neural Network to Pump Card Diagnosis.
- [3] Daphne Cornelisse (2018): An intuitive guide to Convolutional Neural Networks. medium.freecodecamp. Available online at <https://medium.freecodecamp.org/an-intuitive-guide-to-convolutional-neural-networks-260c2de0a050>, updated on 4/24/2018, checked on 10/2/2019.
- [4] Daryl Curtis (2009): Beam Pump Artificial Lift Optimization. Available online at <https://www.slideshare.net/Daryl17/Beam-Pump-Artificial-Lift-Optimization>, updated on 11/1/2009, checked on 7/1/2019.
- [5] Deng, Xinyang; Liu, Qi; Deng, Yong; Mahadevan, Sankaran (2016): An improved method to construct basic probability assignment based on the confusion matrix for classification problem. In Information Sciences 340-341, pp. 250–261. DOI: 10.1016/j.ins.2016.01.033.
- [6] Downhole Diagnostics (2018): Acoustic Fluid Level Surveys. Available online at <https://www.downholediagnostic.com/fluid-level>, updated on 2018, checked on 7/28/2018.
- [7] Sucker rod pumping short course (2018). With assistance of Downhole Diagnosis. Midland, Texas. Available online at http://docs.wixstatic.com/ugd/f8ee70_d4ba77a8b77e40d898037b28bebad23e.pdf, updated on 2018, checked on 7/20/2019.
- [8] Eijaz Allibhai (2018): Hold-out vs. Cross-validation in Machine Learning. medium. Available online at <https://medium.com/@eijaz/holdout-vs-cross-validation-in-machine-learning-7637112d3f8f>, updated on 2/10/2018, checked on 1/20/2019.
- [9] Falah H. Zawahemah (2002): COMMUNICATIONS TECHNOLOGIES FOR SCADA SYSTEMS. Available online at <http://faculty.kfupm.edu.sa/COE/sadiq/proceedings/SEC2002/vol4/P351.pdf>, checked on 2/1/2019.
- [10] Frank P.Kuhl (1981): Elliptical Fourier Features For a closed contour.
- [11] Jason Brownlee (2018): A Gentle Introduction to k-fold Cross-Validation, updated on 5/23/2018, checked on 12/1/2018.

- [12] Joshi, Prateek (2016): Python. Real world machine learning : learn to solve challenging data science problems by building powerful machine learning models using Python / Prateek Joshi [and four others]. Birmingham, UK: Packt Publishing.
- [13] Marco A. D. Bezerra, Leizer Schnitman, M. de A. Barreto Filho (2009): PATTERN RECOGNITION FOR DOWNHOLE DYNAMOMETER CARD IN OIL ROD PUMP SYSTEM USING ARTIFICIAL NEURAL NETWORKS.
- [14] Master Terminal Units (MTU) in SCADA systems (2011). Available online at <http://electricalquestionsguide.blogspot.com/2011/06/master-terminal-units-mtu-in-scada.html>, updated on 6/28/2011, checked on 5/1/2019.
- [15] Matthew Terribile (2017): Understanding Cross Validation's purpos. meduim. Available online at <https://medium.com/@mtterribile/understanding-cross-validations-purpose-53490faf6a86>, updated on 7/29/2017, checked on 2/16/2019.
- [16] Nameer Hirschkind, Jyo Pari, Jimin Khim: Convolutional Neural Network. Brilliant. Available online at <https://brilliant.org/wiki/convolutional-neural-network/>, checked on 10/2/2019.
- [17] Nazi, G. M.; Ashenayi, Kaveh; Lea, J. F.; Kemp, Frank (1994): Application of Artificial Neural Network to Pump Card Diagnosis. In SPE Computer Applications 6 (06), pp. 9–14. DOI: 10.2118/25420-PA.
- [18] Numerical simulation of the sucker-rod pumping system (2014). Available online at https://www.researchgate.net/publication/274264607_Numerical_simulation_of_the_sucker-rod_pumping_system/figures?lo=1, updated on 12/2014, checked on 7/20/2018.
- [19] Rod pumping overview (2018). Available online at <http://infohost.nmt.edu/~petro/faculty/Kelly/413/ROD%20PM.pdf>, updated on 1/6/2018, checked on 1/7/2018.
- [20] Rowlan, Orvel Lynn; Lea, James F.; McCoy, James N.: Overview of Beam Pump Operations. Available online at <https://www.onepetro.org/conference-paper/SPE-110234-MS>.
- [21] Rushin Shah (2014): Image feature extraction. Available online at <https://de.slideshare.net/Jaddu44/image-feature-extraction>, updated on 3/6/2014, checked on 2/15/2019.
- [22] Sarang Narkhede (2018): Understanding Confusion Matrix. /towardsdatascience. Available online at <https://towardsdatascience.com/understanding-confusion-matrix-a9ad42dcfd62>, updated on 9/5/2018, checked on 1/15/2019.

- [23] shruti saxena (2018): Precision vs Recall. towardsdatascience. Available online at <https://towardsdatascience.com/precision-vs-recall-386cf9f89488>, updated on 11/5/2018.
- [24] Sidat Asiri: Meet Artificial Neural Networks. Available online at <https://towardsdatascience.com/meet-artificial-neural-networks-ae5939b1dd3a>, checked on 1/2/2018.
- [25] Suliman, Alaeldin; Zhang, Yun (2015): A Review on Back-Propagation Neural Networks in the Application of Remote Sensing Image Classification. In JEASE 5 (1). DOI: 10.17265/2159-581X/2015.01.004.
- [26] Takács, Gábor (2003): Sucker-rod pumping manual. Tulsa, Okla.: PennWell Corp.
- [27] Takács, Gábor (2015): Sucker rod pump handbook. Amsterdam: Gulf Professional Publishing.
- [28] Wikipedia (2016): Feature extraction, updated on 6/1/2016, checked on 12/2/2019.
- [29] Wikipedia (2019a): Convolutional Neural Network, updated on 1/30/2019, checked on 2/18/2018.
- [30] Wikipedia (2019b): Fault tree analysis. Available online at https://en.wikipedia.org/wiki/Fault_tree_analysis, updated on 2/14/2019, checked on 1/7/2018.
- [31] Wikipedia (2019c): Softmax function. Available online at https://en.wikipedia.org/wiki/Softmax_function, updated on 2/17/2019, checked on 12/2/2019.
- [32] Wikipedia (2019d): Confusion matrix. Available online at https://en.wikipedia.org/wiki/Confusion_matrix, updated on 4/2/2019, checked on 1/28/2019.
- [33] XIE LU (2014): Supervisory Control and Data Acquisition System Design for CO2 Enhanced Oil Recovery, University of California at Berkeley. Available online at <https://www2.eecs.berkeley.edu/Pubs/TechRpts/2014/EECS-2014-123.pdf>.
- [34] ZHANYU GE (1998): STATISTICAL ANALYSIS OF SUCKER ROD PUMPING FAILURES IN THE PERMIAN BASIN, Faculty of Texas Tech University.